Article:
Niaz, T, Sarkar, A orcid.org/0000-0003-1742-2122, Mackie, AR orcid.org/0000-0002-5681-0593 et al. (1 more author) (2021) Impact of albumin corona on mucoadhesion and antimicrobial activity of carvacrol loaded chitosan nano-delivery systems under simulated gastro-intestinal conditions. International Journal of Biological Macromolecules, 169 (2). pp. 171-182. ISSN 0141-8130

https://doi.org/10.1016/j.ijbiomac.2020.12.085

Impact of albumin corona on mucoadhesion and antimicrobial activity of carvacrol loaded chitosan nano-delivery systems under simulated gastro-intestinal conditions

Authors: Taskeen Niaz[c☼], Anwesha Sarkar[☼], Alan Mackie[☼]*, Muhammad Imran[c]*

[c] Department of Biosciences, COMSATS University Islamabad (CUI), Park road, Islamabad, Pakistan

[☼] Food Colloids and Bioprocessing Group, School of Food Science and Nutrition, University of Leeds, Leeds LS2 9JT, UK

*** Corresponding author:**

Dr. Muhammad Imran (m.imran@comsats.edu.pk)

Prof. Dr. Alan Mackie (A.R.Mackie@leeds.ac.uk)

Abstract

Emerging antibiotic resistance in pathogens has posed considerable challenges to explore and examine the natural antimicrobials (NAMs). Due to the labile nature of NAMs, nano-delivery systems (NDS) are required to protect them from physiological degradation and allow controlled delivery to the targeted site of infection. In this study, corona modified NDS were developed using bovine serum albumin (BSA) on a chitosan core (CS) for sustained delivery of carvacrol (CAR), a natural antimicrobial agent, in the intestine. The optimal nano-formulations of the core (CS-NDS) and corona modified (BSA-CS-NDS) systems were fabricated with an average diameter of 52.4±10.4 nm and 202.6±6 nm, respectively. A shift in zeta-potential (ZP) from positive (+21±3.6 mV) to negative values (-18±2.6 mV) confirmed the electrostatic deposition of BSA corona on CS core. Under the influence of various simulated gastrointestinal conditions, BSA corona provided extra stability to NDS (ZP -38.5 mV), by ensuring delayed release and limited degradation in the gastric conditions. Mucoadhesive studies with quartz crystal microbalance with dissipation (QCM-D) revealed that BSA corona reduced the mucoadhesion of NDS at gastric pH, which enabled the effective delivery of CAR to the intestinal phase for successful eradication of *Salmonella enterica*.

Keywords: Chitosan; bovine serum albumin; corona modification; simulated digestion; carvacrol; nano-antimicrobials

1. Introduction

Enteric infections spread by contaminated food account for significant morbidity and mortality worldwide [1]. Among all foodborne enteric pathogens, *Salmonella enterica* serovar *Typhi* has the capacity to invade and interact with intestinal mucosal surface [2]. With the emergence of antibiotic resistance in *Salmonella* strains, more efforts are required to identify and exploit alternative natural antibacterial therapies against *Salmonella* infections.

Essential oils (EOs) are natural compounds, some of which have antimicrobial activities and have been extensively used in pharmaceutical, cosmetics and food industries [3-5]. Among various EOs, carvacrol (CAR) has demonstrated high antibacterial potential [6]. CAR is a terpenoid found in significant concentrations in oregano and thyme essential oils, which is classified as Generally Recognized as Safe (GRAS) by the Food and Drug Administration (FDA, 2016). It has broad-spectrum antimicrobial activity against enteric foodborne pathogens [6, 7]. However, the application of CAR is limited due to several activity-lowering factors including low stability under physiological conditions, high volatility, and low bioavailability in the lower gut [7]. These challenges can be effectively surmounted by encapsulating EOs in the nano delivery systems (NDS) assembled from biodegradable polymers intended for oral intake such as lipids, carbohydrates and proteins [8, 9]. Moreover, nano-encapsulation enhances the stability and controlled release of bioactive agents [8]. Therefore, biodegradable materials have already been reported for the nano-encapsulation of EOs, such as chitosan (CS), dextrin and amylopectin [10-12].

Chitosan is a natural polysaccharide derived from chitin after deacetylation. Owing to its low production costs, biodegradability, biocompatibility and FDA approval, applications of CS in food and pharmaceutical industry have increased remarkably [13-15]. Recent studies on encapsulation of CAR and thymol EOs in chitosan [10, 16, 17] concluded that nano-encapsulation improved its *in vitro* antimicrobial activity and controlled release. However, NDS intended for intestinal delivery to treat enteric infections have to pass through oral and gastric digestion before reaching the targeted intestinal site [18]. The highly mucoadhesive property of CS is disadvantageous in this regard, as CS-NDS will get entrapped in the gastric mucosa and release the active agent before it reaches the target site (intestine).

The formation of a protein layer on polysaccharides could be one potential solution to stabilize and protect CS-NDS from non-targeted release. Core-shell NDS have been employed for the stabilization and fortification of dairy drinks [19-21]. Complex formation between globular proteins such as BSA and β-lactoglobulin (β-Lg) with polysaccharide induces

conformational changes in proteins without affecting their original functional properties [22] and can be used to decrease gastric digestibility of the proteins. Furthermore, increase in steric hindrance and electrostatic interactions induced by protein interaction with polysaccharide may not only impede the aggregation process but also hinder the binding between the pepsin active site and protein [23-25].

In our previous study, core-shell NCS with alternative protein-polysaccharide corona were successfully optimized and characterized (Niaz et al., 2019). In the present study, we have focused on the effect of corona modification (BSA corona) on mucoadhesive property, antimicrobial potential, sustained release and digestive fate of carvacrol loaded chitosan NDS. These findings provide an effective strategy for the treatment of enteric infections caused by foodborne pathogens such as *Salmonella enterica*.

2. Materials and methods

2.1. Chemicals

CAR (5-isopropyl-2-methylphenol CAR, ≥98%), medium molecular weight chitosan (CS) with 85% degree of deacetylation, tripolyphosphate (TPP), bovine serum albumin (BSA) and fluorescein isothiocyanate (FITC) were purchased from Merck, UK. Phosphate buffer saline (PBS) was purchased from Oxoid-Thermo Fisher scientific. Different digestive enzymes *e.g.* Pepsin (P7000-25G, actual activity: 474 U/mg), pancreatin (P7545, trypsin activity U/mg solid: 6.96) and bile salts (B8631-100G) were provided by Merck life sciences, Germany. Crystal violet dye and Sudan red G were purchased from Daejung Chemicals.

2.2. Fabrication of corona modified nano delivery systems

Corona modified CS-NDS was prepared by dissolving 0.3 % (w/v) chitosan in 1% (v/v) acetic acid solution. Afterward, 1 mL of TPP (1% w/v) solution was added dropwise (1 drop/10sec) into 10 mL of chitosan solution while stirring (600 rpm). The solution was allowed to stir for 60 min followed by ultra-sonication for 25 min. For the fabrication of BSA-CS-NDS, BSA solution was prepared by dissolving BSA (50 mg/mL) in 5 mL of 10 mM NaCl solution. Subsequently, pH of the solution was adjusted to 7.0 and it was kept on magnetic stirrer (500 rpm) at room temperature (25°C) for 20 minutes. Finally, to obtain BSA corona on CS core prepared CS-TPP-NDS were added dropwise into the BSA solution and allowed the NDS solution to stir (500 rpm) for 45 min at room temperature. For CAR-loaded NDS, predetermined weight of CAR (final concentration 1 mg/mL) was dissolved in an aqueous solution of chitosan for the respective NDS.

2.3. Quantitative analysis of the carvacrol

Samples were analyzed by gas chromatography coupled with mass spectroscopy (GC–MS) as previously described [26]. The oven temperature was programmed as follows: an initial temperature of 90 °C for 3 min, then increased at a rate of 3 °C min^{-1} to 115 °C, increased again at a rate of 6 °C min^{-1} to 140 °C and finally increased at 40 °C min^{-1} to 200 °C.

A calibration curve was constructed by dissolving various concentrations of pure CAR in ethanol. Quantification of CAR was performed by comparing the chromatographic values of encapsulated CAR with the standard curve while using GC-MS.

2.4. Encapsulation efficiency and loading capacity of carvacrol

The content of CAR in the corona modified NDS was determined following the method of Hou et al. (2012). CAR-loaded NDS samples were centrifuged at 10,000 g (4 °C). After discarding the supernatant, the encapsulated CAR was extracted from the pallet with ethanol. Unknown concentration of CAR was obtained by referring to the standard curve of CAR prepared by GC-MS in section 2.3.

Encapsulation efficiency (EE) was calculated by following the equations below:

$$EE\ (\%) = \frac{Encapsulated\ carvacrol\ in\ NDS\ (peallet)}{Total\ amont\ of\ carvacrol\ added\ in\ the\ NDS} \times 100 \quad \text{(I)}$$

2.4.1. Fourier transform-infrared (FTIR) spectroscopic analysis

FTIR analysis of individual components of nano delivery systems, active agent (CAR), void and CAR-loaded NDS were carried out by using an FTIR spectrometer (Thermo Fisher Scientific, Waltham, MA) by KBr pellet method in the wavelength range of 4000–500 cm^{-1} [27].

2.5. Particle size, polydispersity index (PDI) and zeta-potential

The physicochemical properties of corona-modified NDS (void and CAR-loaded) were compared to understand the fate of these NDS before and after passing through the simulated oral, gastric, and small intestine conditions. The mean particle size and polydispersity index (PDI) were measured using dynamic light scattering and zeta potential of the NDS was assessed using capillary electrophoresis, both with Zetasizer ZS (Malvern, UK). Briefly, 50 μL of samples were diluted in 800 μL of deionized H_2O in 1 mL cuvette (or folded DTS1070 capillary

electrophoretic cell for zeta-potential) and measured at 25 °C, with a refractive index of 1.523. Each sample was measured in triplicate and the average values were used [28, 29].

2.6. Morphology of core-corona NDS

The morphological changes of the void and CAR-loaded BSA-chitosan-based core-corona modified nano delivery systems (NDS) were investigated using Field Emission Scanning electron microscopy (FE-SEM) (Tescan, USA) as described previously by Niaz *et al*., 2018 [27]. Briefly, about 5 µL of NDS solution was spread on a glass slide (1 × 1 cm) and let it dry at room temperature. Air-dried samples were sputter-coated with gold and SEM was performed under electron acceleration voltage of 5–10 KeV.

2.7. *In-vitro* digestion with INFOGEST protocol

In-vitro digestion experiments were performed according to the standardized static *in-vitro* digestion method by Minekus *et al*, 2014. Simulated gastric and intestinal phase digestion steps were performed on both void and loaded-core CS-NDS as well as on BSA-CS core-corona NDS as described by [30] with minor modifications. Samples taken before and after gastric and intestinal phase were stored at −80 °C until further preparation or analysis. Sampling in oral phase was not performed because beverages and liquids have short exposure time to oral conditions [31]. Simulated salivary fluid (SSF), simulated gastric fluid (SGF) and simulated intestinal fluid (SIF) were prepared accordingly [32]. Enzyme solutions used in each phase were prepared in their corresponding electrolyte stock solutions (SSF, SGF or SIF). Simulated digestion of the void and CAR loaded BSA-CS-NDS were performed with or without skim milk (used as food). Digestion without any nano-formulation was performed as control. Sampling was performed (500 µL) in both gastric and intestinal phases at each time point e.g. 2, 5, 10, 20, 30, 60 minutes.

2.7.1. Simulated oral digestion

To start simulated digestion, electrolyte stock solution of SSF (4 mL) was mixed with 5 mL of skim milk (mixed with 0.1% nano-formulations just before the start of the digestion) in a 50 mL falcon tube. Subsequently, 975 µL of dH_2O and 25 µL of $CaCl_2$ (0.3 M) were added into the tube and pH was adjusted to 7. Finally, the mixture was incubated in a shaking incubator (S1900R, Robus Technologies, UK) at 37 °C and 100 rpm for 2 minutes.

2.7.2. Simulated gastric digestion

After the oral digestion, electrolyte stock solution of SGF (6.4 mL, pH 3) was added to the 10 mL oral bolus. Afterwards, 1.6 mL of pepsin (40,000 U) prepared in SGF was added, followed by the addition of 5µL of 0.3 M $CaCl_2$ in a falcon tube, pH of the SGF was adjusted to 3 with 1M HCl solution. Finally, 0.923 mL of deionized water was incorporated. Hence, a final ratio of oral bolus to SGF of 50:50 (v/v) was obtained. Lastly, the mixture was incubated in a shaking water bath at 37 °C at 100 rpm for 1h.

2.7.3. Simulated intestinal digestion

Following the gastric digestion, 11 mL of SIF based electrolyte stock solution was mixed with remaining gastric chyme (17 mL). Then, 2.5 mL of fresh bile solution (prepared in deionized water) and 40 µL of 0.3 M $CaCl_2$ were added to the falcon tube. 1 M NaOH (0.7 mL) was used to adjust the pH of intestinal phase at 7. Afterwards, 5 mL of pancreatin solution (4,000 U trypsin activity) prepared in SIF was taken and 0.796 mL of deionized water was also added to make final ratio of gastric chyme to SIF 50:50 (v/v). Finally, the mixture was placed in the shaking water bath at 37 °C and 100 rpm for 1 h. The pH of the intestinal phase was monitored throughout the digestion and maintained at pH 7 using 1 M HCl or 1 M NaOH solutions.

2.8. Release of carvacrol from corona modified nano-systems during digestion

During *in vitro* digestion, the samples taken were centrifuged at (10,000 g at 4 °C) for 45 min. Nano-systems were separated as a sediment phase at the bottom, a clear supernatant in the middle and upper micellar layer was collected. CAR in the micellar layer was extracted in ethanol and quantified using GC-MS as described in section 2.3. Release percentage of CAR during digestion was calculated by using the formula as given below

$$\%\ \text{Release of carvacrol} = \frac{Amount\ of\ carvacrol\ in\ the\ supernatant}{Total\ amount\ of\ carvacrol} \times 100 \quad \text{(III)}$$

2.9. Mucoadhesive potential of corona modified nano-systems using quartz crystal microbalance with dissipation QCM-D

Interaction of CS-NDS and corona modified CS-BSA-NDS with the gastric mucin at different pH values (to mimic oral, gastric and intestinal phase) were performed using E4 system, Q-Sense, Biolin Scientific Sweden. Gold-covered quartz crystals (QSX-301, Q-Sense) were used. All experiments were conducted at 37 ± 0.1 °C using a flow rate of 0.11 mL/min in a flow mode. Experiment was performed as described previously by Oh et al., 2016 [33, 34] with slight modifications. Briefly, phosphate buffer saline (PBS) was injected into the flow cell to

allow a stable baseline. After stabilization of the signals, porcine gastric mucin (0.025 % in buffer) was introduced to the crystal until both resonance frequency Δf and dissipation ΔD stabilized, after that buffer was introduced for 15 min to remove any unbound mucin [35]. After establishing a stable mucin base layer, individual polymers and nano-formulations (0.1 %) prepared in the buffer at different pH were introduced to the QCM-D chamber. The data were fitted using Voigt model for viscoelastic materials (namely, "Smartfit Model") by Dfind (Q-Sense, Sweden) software to obtain the adsorbed mass of the samples (Xu et al., 2020). The 3rd to 11th overtones were considered for data analyses.

2.10. Antimicrobial potential of nano-formulations

To assess the antimicrobial potential of released amount of CAR from core and corona-modified NDS during digestion, S*almonella enterica* (1×10^5 CFU/mL) was exposed to equal volume of digesta (digested samples of core and corona-modified NDS) extracted at different time points in 96-well plate, this method is adopted and modified from previous microdilution methods [27, 36-38]. Plates were incubated overnight at 37 °C. After 24 h, optical density values of inoculated broth containing digesta (with released CAR) were recorded at 600 nm in spectrophotometer (Multiskan GO - Thermo Scientific). Inoculated broth without any digesta samples were considered as control positive. Bacterial growth inhibition was determined by change in optical density/turbidity. Each sample was measured in triplicate and the average values with ± SD were plotted. Statistical analysis (one-way ANOVA or Student T-test) was performed to measure statistical significance between the core and corona modified NDS at different time intervals.

2.11. Cytotoxicity analysis by MTT assay

To determine the cytotoxic effect of free and encapsulated carvacrol in core as well as corona modified nano delivery system (NDS), MTT (3-(4,5-dimethylthiazol-2-yl)-2,5-diphenyl tetrazolium bromide) assay was performed as described previously by Shinde et al., 2020 [39]. Briefly, 15000 cells/well were seeded in 96 well plate and were incubated in the presence of free CAR, CAR loaded core CS-NDS (CAR-CS-NDS) and CAR loaded corona modified NDS (CAR-BSA-CS-NDS) at the concentrations of 1.56, 3.12, 6.25, 12.5, 25 and 50 µg/mL for 24 h. Post-treatment media was removed, cells were treated with 5 mg/mL of MTT reagent and incubated at 37 °C in a CO_2 incubator for 4 h to produce dark blue colored formazan crystals. Finally, the crystals were dissolved in 150 µL of Dimethyl sulfoxide (DMSO) and absorbance was noted at 570 nm in multiplate spectrophotometer.

2.12. Statistical analysis

All experiments were carried out in triplicates. The results were expressed as mean ± standard deviation (SD) of three independent experiments. Statistical analysis of the data was performed by Graph pad prism (version 7.0) by applying one-way ANOVA and Student T-test. p values < 0.05 were considered as statistically significant.

3. Results and discussion

3.1. Characterization of the nano delivery systems

Particle size, zeta potential, polydispersity index (PDI) and encapsulation efficiency (%EE) are vital considerations for designing a delivery system of bioactive compounds. In theory, the ideal characteristics of NDS are nanometer size with lowest PDI value, high zeta potential and high %EE [40]. Figure 1 shows the effect of corona layer on the %EE and physicochemical properties of CS-NDS.

The particle size of the void CS-NDS was found to be 52.4±10 nm, which increased after encapsulation of CAR to 163±4 nm (Figure 1-A). Similarly, an increase in the particle size was observed with BSA-corona formation around the core of CS in the core-corona NDS with hydrodynamic diameter of 202±6 nm. Particle size further increased to 445±3 nm after encapsulation of CAR in BSA-CS-NDS (Figure 1-A). This increase in size might have occurred due to the slight repulsion between CAR and TPP which was used as cross-linker in CS-NDS (both are anionic in nature). Furthermore, CAR binds with positively charged CS and entrapped between the polymer network, which resulted in the bigger size of CAR-loaded NDS. In BSA-CS-NDS, CAR also adsorbed onto the surface of NDS i.e. BSA corona by hydrophobic interactions which further increase the size of these NDS.

These results coincide with the previous studies where increase in particle size was observed after the formation of protein or polymer corona around CS nano-systems [41, 42]. The PDI of all nano-formulations were ≤ 0.3 except for CAR-CS-NDS, which was slightly higher (0.38). This indicated that the particle size of CS-NDS was not as homogenous as other nano-formulations, which was also consistent with the SEM results (Figure 2).

The ZP of void CS-NDS was +21±3.6 mV, which was reduced to -18±2.6 mV after electrostatic deposition of BSA on CS-core (Figure 1-B). The observed shift in ZP from positive to negative confirmed the formation of mutually oppositely charged BSA-corona on the CS-core. After encapsulating CAR in core-corona NDS, reduction in zeta potential of CS-

NDS to 16±5.84 mV and increase in zeta-potential of BSA-CS-NDS to -21.9±3.1 mV was observed. This might be attributed to the anionic nature of CAR confirming binding [43]. Higher zeta potential (positive or negative) values generate the stability of nano-formulations. As stated previously, NDS with ZP of ±10–20 mV, ±20–30 mV and > ±30 mV are considered as relatively stable, moderately stable and highly stable, respectively [44]. Hence, it can be concluded that the encapsulation of carvacrol in corona modified NDS further enhanced the colloidal stability of the particles (as increase in ZP from -18±2.6 mV to -21.9±3.1 mV was observed) and prevented them from aggregation, which can be seen in SEM results (Figure 2) as well. However, in case of unmodified CS-NDS, encapsulation of carvacrol slightly reduced the ZP from +21±3.6 mV to 16±5.84 mV, which indicated lower particle stability of CS-NDS.

To determine the retention of CAR while passing through GIT after oral administration of corona modified NDS, EE% was measured at various pH values *i.e.* pH 7.0, 5.0 and 3.0. The %EE of CAR at pH 7.0, 5.0 and 3.0 in CS-NDS was 51±6.8%, 68±1% and 75±1.5%, respectively (Figure 1-C). This might be due to the reduced interaction between oppositely charged TPP and CS with increase in pH from pH 3.0 to pH 7.0. Chitosan at relatively low pH (pI < 6.5) is positively charged and tends to be soluble in the aqueous solutions. Nevertheless, at higher pH, it may precipitate from the solution due to deprotonation of the amino groups [45], which resulted in lower %EE of active agent at higher pH value. On the other hand, after the formation of BSA corona on CS-NDS, overall increase in %EE of CAR was observed *i.e.* 73±2%, 93±1% and 85±1.2% at pH 7.0, pH 5.0 and pH 3.0, respectively. Another reason behind higher %EE of CAR in BSA-CS-NDS is the presence of charged amino groups in the BSA structure, which allow the electrostatic adsorption of anionic molecules like CAR [46]. Furthermore, due to its hydrophobic character, CAR can also entrapped in the hydrophobic domains of BSA-corona [47]. Therefore, higher %EE could be achieved when BSA is used as a corona around the core of nano-systems.

3.2. Morphological studies

Scanning electron micrographs (SEM) showed the morphology of the void and CAR-loaded core-corona NDS (Figure 2). The individual CS-NDS showed spherical shape with an average size of 80-100 nm, which is within the range expected from the dynamic light scattering (DLS) data (Figure 1-A). However, some partially aggregated particles were also visible, which might have been caused during sample preparation for SEM [48]. SEM of the CAR-loaded chitosan NDS (CAR-CS-NDS) displayed spherical shape with larger particle size (100-120 nm) when

compared with void NDS in line with the DLS data (Figure 1-A). It was observed that after CAR loading, CS-NDS appeared to be well-separated and stable over the various steps of sample preparation for the SEM analysis. Similarly, corona-modified (BSA-CS) NDS (Figure 2-IV) appeared to be homogeneous with spherical morphology and larger in size than core chitosan nano-systems. Moreover, entrapment of CAR in BSA-CS-NDS did not affect the morphology of particles, although size of these NDS increased up to 400nm (Figure 2-V) as compared to the void NDS (200nm), which validates entrapment of CAR in the delivery systems [49]. Slight agglomeration in CAR-loaded NDS was also observed, due to the presence of some CAR at the particle surface, which might have promoted bridging between adjacent NDS. These results are in accordance with previous results where essential oil-loaded CS nano-systems demonstrated spherical and smooth morphology with some degree of agglomeration [38, 50].

3.3. Fourier transformed infrared (FTIR) spectroscopy

Fourier transformed infrared (FTIR) spectroscopy was used to confirm BSA corona formation on CS-NDS as shown in Figure 3-I. The spectrum of chitosan exhibited a strong and broad band at 3433 cm^{-1} which represents overlapping due to H-bonding of the O-H and N-H stretching vibrations. FTIR spectral peaks appeared at 2923 cm^{-1}, which belonged to symmetric and asymmetric CH_2 bending vibrations of carbohydrate ring in CS polymer. Characteristic polysaccharide bands from C=O stretching of amide I, N–H bending and C–N bending corresponding to amide II (vibrational mode) group could be observed at 1651 cm^{-1} and 1381 cm^{-1} respectively. Peak at 1069 cm^{-1} represents pyranose ring structure [51-53]. In FTIR spectral image of CS-NDS (Figure 1, supplementary data), broad band of N-H and O-H stretch at 3433 cm^{-1} shifted to 3442 cm^{-1}, which confirmed the disruption of H-bonding by crosslinking with TPP. Shifting of amide I peak from 1651 cm^{-1} to 1633 cm^{-1} and disappearance of amide II in CS–NDS confirmed the conformational changes in CS polymer and formation of CS-NDS [52].

The FTIR spectra of BSA powder demonstrated O–H, C-H and –C=C– alkynes stretch at 3313, 2928 and 2109 cm^{-1}, respectively [54]. Bands appear at 1600-1700 cm^{-1} associated with the secondary structure and conformation of proteins. After formation of BSA corona/shell on CS-NDS (Figure 3-I), merging of 1657 and 1534 cm^{-1} and a sharp characteristic vibrational peaks of proteins appeared at 1641 cm^{-1} representing BSA corona on CS-NDS [55]. Shifts in these peaks from individual polymers confirmed the electrostatic

interaction between COO^-, NH^3 and OH^- group of BSA and CS to form BSA corona on CS-NDS.

The IR spectrum of CAR presented the characteristic bands at 3403 cm^{-1} and 2961 cm^{-1} corresponding to wide vibrational phenolic (O-H) group and C-H stretching, respectively. Intense peaks at 1590 cm^{-1} and 1503 cm^{-1} corresponding to the presence of aromatic C=C stretching vibrations were also observed [56, 57]. Moreover, the presence of a peak at 1422 cm^{-1} corresponds to the isopropyl group and a strong band in 1252 cm^{-1} is due to C-O stretching vibration. Peaks observed at 995 cm^{-1} and 938 cm^{-1} corresponds to aromatic C-H bending [58], which can be attributed to aromatic ring substitution of CAR (Figure 3-III).

In the FTIR spectrum of CS-NDS, the key characteristics peak appearing at 3438 cm^{-1} represented the H-bonding of O-H and N-H stretching vibrations. Similarly, IR signals appearing at 2914 cm^{-1} indicated the symmetric and asymmetric C-H stretching vibrations of carbohydrate ring and 1632 cm^{-1} represented the C=O stretching, N–H bending and C–N stretching from amide I and amide II groups present in CS polysaccharide [59]. After the addition of carvacrol in CS-NDS, the intensity of the O-H and C-H stretching peak at 2914-3438 cm^{-1} increased significantly (Figure 3-II), which reflected the incorporation of carvacrol in the chitosan matrix. Thus, the C-H stretching peak can be used as a probe for the determination of carvacrol loading in the NDS. Furthermore, the appearance of small peaks at 1270 cm^{-1} and 1039 cm^{-1} (which represented the C-O stretching vibration and aromatic C-H bending stretch of carvacrol aromatic ring) were also observed in the CAR-CS-NDS, which also confirmed the presence of carvacrol on the surface of CS-NDS [56].

Similarly, FTIR spectra of the corona modified NDS obtained after the addition of CAR were almost similar to that of void NDS. However, decrease in wavenumber of C-H vibrational peaks from 3403 cm^{-1} to 3395 cm^{-1} and appearance of a sharp signal at 1634 cm^{-1} corresponding to Amide I, Amide II and secondary structural conformation changes in protein corona resulted from absorption and loading of CAR. These results confirm the formation of BSA corona on CS-core by isoelectric interactions between COO^-, NH^3 and OH^- group of BSA and CS. Additionally, FTIR results displayed that CAR molecules were not only entrapped in the CS-NDS matrix but were also absorbed in the BSA layer in corona modified NDS.

3.4. Gastrointestinal fate of core-corona modified nano-delivery systems

After initial characterization, the NDS were exposed to simulated GIT conditions that included gastric and small intestine phases. Changes in particle size and zeta-potential were recorded to evaluate the fate of CAR-loaded corona-modified NDS under GIT conditions (Figures 4 and 5).

Simulated gastric phase. The particle size, PDI and zeta-potential of corona-modified and unmodified NDS changed significantly after entering gastric phase as compared to the initial sample (Figure 1-A). The particle size distribution was not affected much during gastric digestion of the void CS-NDS (Figure 4A-I). Zeta potential of CS-NDS remained between 20 to 25 mV (Figure 5-I) during the gastric digestion indicating that the amino groups of the chitosan polymer remained deprotonated and positively-charged in the simulated gastric pH and interacted with the negatively-charged TPP due to the electrostatic interaction, which resulted in stable NDS [28]. However, CAR-loaded NDS demonstrated heterogeneous size distribution (Figure 4A-II) and low zeta-potential (13 mV) during gastric phase, thus representing lower stability of CAR-CS-NDS (Figure 5-II) as compared to void CS-NDS.

When NDS with a BSA corona were subjected to gastric digestion, size distribution was skewed towards right in both void and CAR-loaded NDS (Figure 4B (I, III)). This trend could be due to change in the level of protonation of BSA corona at pH < 4.0 [59]. Reduction in zeta-potential values of void corona-modified NDS from -25.9 mV to almost -20 mV confirmed the stability of these NDS during gastric digestion. Previous studies showed that NDS with ZP ±20 to ±30 mV are considered as moderately stable and with ZP > ±30 mV are deemed as highly stable [60]. However, increase in the size of NDS in this phase could be due to partial unfolding and protonation of the BSA at low pH. As reported previously, average molecular size of BSA was increased from 10.1±0.5 nm to 12.4±0.6 nm with a decrease in pH value [61]. It was also observed that BSA had a partially unfolded structure at a pH lower than its isoelectric point (pI 4.7), which resulted in less compressibility of BSA corona and ultimately increased the size of BSA-CS-NDS. Furthermore, decrease in pH from 7.0 to 4.7 reduced the negative charge on BSA, as partial unfolding exposed more basic amino acid residues, thus more hydrophobic groups of the BSA molecule were accessible to ionization at low pH [59]. Net positive charge on BSA is increased at pH < 4.0 [62]. Thus, our results suggested that BSA will slightly change its conformation in the gastric phase which would affect the surface charge and size of corona modified NDS. Overall, BSA-CS-NDS remained stable with conserved characteristics of the nano-system during gastric digestion. Zeta-potential values of CAR-loaded corona-modified NDS remained higher (-38.5 mV to -43.8

406 mV) than void NDS, thus confirming a higher stability of CAR-loaded NDS during the gastric
407 phase. Owing to its hydrophobic nature, CAR would entrap in the hydrophobic domains of
408 BSA, hence less hydrophobic groups will be available for ionization of BSA at low pH, which
409 provided extra stability to the nano-systems.

410 **Simulated intestinal phase.** After entering into the simulated intestinal phase, the peak of the
411 particle size distribution of the void CS-NDS decreased (Figure 4, A-II), while illustrating a
412 bimodal size distribution and a peak population at around 10 μm appeared, possibly due to the
413 digestion of CAR-CS-NDS by pancreatin (Figure 4, A-IV). ZP measurements demonstrated
414 the charge of CAR-CS-NDS approaching to zero during initial 10 minutes of intestinal
415 digestion and then becoming negative (Figure 5-II). This observation suggested the degradation
416 and dissociation of CS-NDS at pH 7.0 (intestinal pH) as well as burst release of anionic CAR
417 at this stage. These results coincide with previous studies where chitosan-NDS remained stable
418 in gastric environment while degradation and aggregation was observed in intestinal pH with
419 a burst release of the encapsulated active agent [63, 64].

420 The size distribution of CAR-BSA-NDS in the intestinal phase was broad and
421 multimodal with appearance of both small and large particles during the first 10 minutes of
422 intestinal digestion (Figure 4, B-IV). Subsequently, a bimodal size distribution shifted towards
423 1000 nm size was observed. This suggests the complete digestion of BSA corona by pancreatic
424 trypsin, thus resulting in the degradation of NDS. Zeta potential of void corona modified NDS
425 was reduced to zero (from negative) during first 20 minutes and turned towards positive during
426 the next 40 minutes of intestinal digestion. Similarly, zeta potential values approached to zero
427 at the end of intestinal digestion for CAR-BSA-CS-NDS. These results suggested that the
428 gradual degradation of BSA corona could expose the core of NDS (CS core), which would start
429 swelling and degrading with gradual release of CAR from NDS as chitosan began losing its
430 positive charge once exposed to the intestinal pH.

431 **3.5 Release profile of carvacrol**

432 To explore the release behavior of encapsulated CAR in core and corona-modified
433 nanosystems, *in vitro* release profiles were measured under simulated gastrointestinal
434 conditions (Figure 6). *In vitro* release profiles of CAR from CS-NDS are shown in Figure 6-I.
435 The presence of CAR in the micellar phase was only 20% after 20 min in SGF digestion.
436 However more pronounced burst release of CAR was observed after 10 min of incubation in

SIF, whereas almost 76% of CAR release was detected in SIF after 30 min. This indicated the dissolution of chitosan nano-structures due to phase shift from SGF to SIF (pH 2 to 7.4).

The formulation of CAR-loaded corona-modified (CAR-BSA-CS) NDS revealed only 10% of CAR release during 60 min incubation in SGF. However, core-corona NDS provided sustained release (30%) during initial 20 min in the intestinal phase. Thus, as compared to SGF, higher release of CAR in SIF might be due to the high degree of proteolysis of BSA corona on the core of CS-NDS by trypsin in intestinal phase. While in SGF (at acidic pH), limited digestion of BSA by pepsin allowed relatively less release of CAR molecules, which were trapped in the hydrophobic pockets of BSA layer [59]. From release kinetics observations, we can conclude that BSA corona formation on CS-NDS hinders CAR release in the stomach and allows its release in the later phase (intestinal phase), thus making it available in active-form for the successful eradication of enteric pathogens. These results are consistent with the previous findings of Dai *et al*., who proposed that protein-based nanoparticles could protect most of the phenolic active agent from being released in the stomach and controlled its release later in the small intestine [65].

3.5. QCM-D analysis: Mucoadhesive potential of corona modified nano-delivery systems

Quartz crystal microbalance with dissipation monitoring (QCM-D) was used to investigate the mucoadhesive properties of CAR-loaded CS-NDS with or without BSA corona at optimization and gastrointestinal pH conditions *i.e.* pH 3.0, 5.0 and 7.0 (Figure 7). Generally, changes in "*f*" are qualitatively related to negative or positive mass change in the system, either by desorption or adsorption (Xu et al., 2020). On the other hand, changes in "*D*" are qualitatively related to viscoelastic properties of the adsorbed layer, either it is viscous (increase) or rigid (decrease). The Δf and ΔD are shown for 5^{th} overtone. Firstly, the real-time adsorption of porcine gastric mucin (PGM) onto gold-coated sensor was evaluated. As it can be observed from Figures 7(AI-II), gastric mucin adsorbed onto the gold-coated sensors with Δf ~ 15 HZ and an ΔD ~ 3 ppm. Once the mucin layer adsorption was completed, buffer was used to remove unbounded mucin (if any) by rinsing. Since such buffer rinsing induced no changes in the resonant frequency (*f*) and the dissipation factor (*D*) in Figures 7A, suggesting generation of a stable mucin surface coating of 10-15 mg/ m^2 (see Figures 7B) simulating the mucus-coated gastric epithelium. Change after the addition of corona-modified and CS-core nanosystems to the mucin-coated surfaces with changes in adsorbed masses are also shown in Figures 7.

Introduction of CS-NDS at pH 3.0 resulted in a large decrease in *f* and a large increase in *D* (Figure 7A-I). These results indicated a significant increase in adsorbed mass and viscoelasticity. These results confirmed the previous results for the mucoadhesive properties of chitosan. Being a cationic polymer, CS can interact with the anionic sialic and sulfonic acids of the mucus layer through strong electrostatic interactions [66, 67]. Positive charge on chitosan increases at pH below its isoelectric point (pH 5.5) [68, 69]. As the pH increases, deprotonation of amine groups starts, which results in reduced positive charge on chitosan. Hence, at gastric pH, molecular attraction forces by electrostatic interaction of cationic chitosan with negatively charged mucin increased. This is in accordance with the results described in the literature [70, 71] for the significantly improved mucoadhesion properties of chitosan NDS at gastric pH.

Corona modification around CS-NDS provided similar behavior of decrease in *f* and increase in *D* after addition of the mucin layer. However, changes in Δf and ΔD were much smaller for corona-modified NDS than for chitosan-NDS at pH 3.0, indicating less adsorption of BSA-CS-NDS onto the mucin film. These results could be easily interpreted with the change in the mass of corona modified and unmodified NDS at gastric pH, as almost 80 mg/m^2 of mass was increased after adsorption of CS-NDS. Whereas nearly 37 mg/m^2 of mass change was observed in case of BSA-CS-NDS (Figure 7B), which is significantly lower than CS-NDS ($p<0.0001$).

This phenomenon was expected as BSA-CS-NDS had slight interaction with the mucin film due to the electrostatic repulsion of the anionic BSA-CS-NDS with the similarly charged mucin. As overall charge on corona modified NDS, with or without CAR, remained above -20 mV during the whole phase of gastric digestion (Figure 5-III). These results are in agreement with those obtained by Niaz et al., where protein coating reduced the mucoadhesion of chitosan NDS with mucus layer during ex-vivo analysis [60]. We can conclude from QCM-D data that corona modification of CS-NDS with BSA can reduce the mucoadhesive potential of CS-NDS, which allowed the NDS to pass through the gastric phase (without being trapped in the mucus layer) into the intestinal phase. Therefore, encapsulated CAR will finally be released in the intestinal phase for the effective treatment of enteric pathogens e.g. *Salmonella enterica*.

3.6. Antimicrobial potential of carvacrol encapsulated in corona modified NDS

To assess the antimicrobial capability of free and released CAR in the digesta from CAR-loaded corona modified and core-CS NDS, samples of digesta were taken after regular time interval and tested against enteric pathogen i.e. *Salmonella enterica*. Antimicrobial analysis

revealed that free carvacrol was unable to control the growth of enteric pathogen even after 5 min of intestinal digestion. This can be attributed to the low solubility and bioaccessibility of natural phenolic compounds e.g. carvacrol in free form [72]. In comparison with free, CAR released from core-CS NDS were able to control *Salmonella enterica* growth initially, due to the burst release of CAR from CS-NDS when transferred from gastric to intestinal pH (acidic to neutral). However, after 5 minutes of intestinal digestion (Figure 8), continuous increase in the bacterial growth was observed. It might be due to the unavailability of active CAR (after burst release from CS-NDS) to interact with bacterial cells [73]. On the other hand, corona-modified NDS loaded with CAR (CAR-BSA-CS-NDS) exhibited significant control against *Salmonella enterica*, as continuous reduction of bacterial growth was observed after 10 minutes. These results can be explained with the release profile of CAR from BSA-CS-NDS during gastrointestinal digestion. Sustained release of CAR in the intestinal phase from corona modified NDS improved the bioactivity of CAR. CAR micelles released during intestinal digestion (lipolysis and solubilization of CAR by bile salts) [35, 74] would interact with bacterial membrane, which can alter the molecular packing characteristics of phospholipid molecules present in it, thus disrupting the bacterial cell membrane which will result in bacterial cell death [75]. We can conclude from these results that corona modification of CS-NDS with BSA can protect chitosan from pH shock and consequently burst release of CAR in intestinal phase would make corona-modified NDS a promising candidate for the treatments of intestinal infections associated with enteric pathogens.

3.7. Cytotoxicity analysis by cell viability (MTT) *assay*

To assess the cytotoxic effect of free and encapsulated CAR, HepG2 cells were exposed to CAR, CAR-CS-NDS and CAR-BSA-CS-NDS at different concentrations (1.56, 3.12, 6.25, 12.5, 25 and 50 µg/mL) to determine their effects on cell viability (Figure S1). Cell viability decreased significantly when cells were exposed to the higher concentration of free CAR i.e. 25 and 50 ug/mL, as compared to nano-encapsulated CAR in both core and corona modified NDS ($p < 0.01$ and $p < 0.001$). These observations suggested a dose-dependent cytotoxic effect of carvacrol, owing to its antiproliferative and apoptotic inducing properties at higher concentrations [76]. However, no major effect on cell viability (> 90 % cells were viable) was observed after treatment with CAR-CS-NDS and CAR-BSA-CS-NDS, which revealed that encapsulation of CAR in biodegradable and biocompatible material based NDS e.g. BSA and CS reduced its cytotoxic effect due to the controlled release of active agent.

4. Conclusions

This work has provided pertinent information for the intestinal delivery of CAR by corona modified CS NDS; while elucidating the stability, controlled release, mucoadhesion and antimicrobial efficacy during *in-vitro* digestion for the potential treatment of enteric infection associated with foodborne pathogen (*Salmonella enterica*). Our results revealed that corona modified NDS demonstrated higher encapsulation efficiency of CAR and were more stable than unmodified CS-NDS during gastrointestinal digestion. Furthermore, BSA corona formation reduced the mucoadhesion of CS-NDS to gastric mucosa, which reduced the off-target release of CAR in the stomach. Thus, higher release of CAR was facilitated in the intestinal phase without any burst effect. *In vitro* activity of digesta withdrawn at different intervals revealed that corona modified NDS allowed successful control of the growth of *Salmonella enterica* in the intestine. Henceforth, to understand better the structure-activity relationship of nano-antimicrobials in the presence of food *in vivo*, trials should be conducted to expand the applications of food-grade nano-antimicrobials.

Acknowledgement

The authors are grateful to Higher Education Commission (HEC), Pakistan for funding during IRSIP Vide Letter No. 1-8/HEC/HRD/2017/8168 and for the National Research Program for Universities (NRPU) Vide Grant No. 20-4260/R&D/HEC/14/127.

Declaration of competing interest

The authors declare that there is no conflict of interest regarding the publication of this article.

References

[1] J.L. Forbester, D. Goulding, L. Vallier, N. Hannan, C. Hale, D. Pickard, S. Mukhopadhyay, G. Dougan, Interaction of Salmonella enterica serovar Typhimurium with intestinal organoids derived from human induced pluripotent stem cells, Infection and immunity 83(7) (2015) 2926-2934.

[2] E.C. Martens, M. Neumann, M.S. Desai, Interactions of commensal and pathogenic microorganisms with the intestinal mucosal barrier, Nature Reviews Microbiology (2018) 1.

[3] M. Fadli, J.-M. Pagès, N.-E. Mezrioui, A. Abbad, L. Hassani, Artemisia herba-alba Asso and Cymbopogon citratus (DC.) Stapf essential oils and their capability to restore antibiotics efficacy, Industrial crops and products 89 (2016) 399-404.

562 [4] N. Mahato, K. Sharma, R. Koteswararao, M. Sinha, E. Baral, M.H. Cho, Citrus essential
563 oils: Extraction, authentication and application in food preservation, Critical Reviews in Food
564 Science and Nutrition 59(4) (2019) 611-625.
565 [5] L. Marrot, J. Soeur, Use of essential oil of oregano or of rosewood, or constituents thereof,
566 in the cosmetic treatment of keratoses, Google Patents, 2018.
567 [6] L. Marinelli, A. Di Stefano, I. Cacciatore, Carvacrol and its derivatives as antibacterial
568 agents, Phytochemistry reviews 17(4) (2018) 903-921.
569 [7] J.B. Engel, C. Heckler, E.C. Tondo, D.J. Daroit, P. da Silva Malheiros, Antimicrobial
570 activity of free and liposome-encapsulated thymol and carvacrol against Salmonella and
571 Staphylococcus aureus adhered to stainless steel, International Journal of Food Microbiology
572 252 (2017) 18-23.
573 [8] M. Sotelo-Boyás, Z. Correa-Pacheco, S. Bautista-Baños, Y. Gómez y Gómez, Release
574 study and inhibitory activity of thyme essential oil-loaded chitosan nanoparticles and
575 nanocapsules against foodborne bacteria, International Journal of Biological Macromolecules
576 103 (2017) 409-414.
577 [9] J. Hussein, M. El-Banna, K.F. Mahmoud, S. Morsy, Y. Abdel Latif, D. Medhat, E. Refaat,
578 A.R. Farrag, S.M. El-Daly, The therapeutic effect of nano-encapsulated and nano-emulsion
579 forms of carvacrol on experimental liver fibrosis, Biomedicine & Pharmacotherapy 90 (2017)
580 880-887.
581 [10] A. Shetta, J. Kegere, W. Mamdouh, Comparative study of encapsulated peppermint and
582 green tea essential oils in chitosan nanoparticles: encapsulation, thermal stability, in-vitro
583 release, antioxidant and antibacterial activities, International journal of biological
584 macromolecules 126 (2019) 731-742.
585 [11] F. Silva, F. Caldera, F. Trotta, C. Nerín, F.C. Domingues, Encapsulation of coriander
586 essential oil in cyclodextrin nanosponges: A new strategy to promote its use in controlled-
587 release active packaging, Innovative Food Science & Emerging Technologies (2019) 102177.
588 [12] C. Liu, M. Li, N. Ji, J. Liu, L. Xiong, Q. Sun, Morphology and characteristics of starch
589 nanoparticles self-assembled via a rapid ultrasonication method for peppermint oil
590 encapsulation, Journal of agricultural and food chemistry 65(38) (2017) 8363-8373.
591 [13] N. Morin-Crini, E. Lichtfouse, G. Torri, G. Crini, Applications of chitosan in food,
592 pharmaceuticals, medicine, cosmetics, agriculture, textiles, pulp and paper, biotechnology, and
593 environmental chemistry, Environmental Chemistry Letters (2019) 1-26.
594 [14] T.J. Gutiérrez, Chitosan applications for the food industry, Chitosan: derivatives,
595 composites and applications. Wiley-Scrivener Publisher (2017) 185-232.

[15] Z. Shariatinia, Pharmaceutical applications of chitosan, Advances in colloid and interface science 263 (2019) 131-194.
[16] K. Yao, W. Chen, F. Song, D.J. McClements, K. Hu, Tailoring zein nanoparticle functionality using biopolymer coatings: Impact on curcumin bioaccessibility and antioxidant capacity under simulated gastrointestinal conditions, Food Hydrocolloids 79 (2018) 262-272.
[17] E. Medina, N. Caro, L. Abugoch, A. Gamboa, M. Díaz-Dosque, C. Tapia, Chitosan thymol nanoparticles improve the antimicrobial effect and the water vapour barrier of chitosan-quinoa protein films, Journal of Food Engineering 240 (2019) 191-198.
[18] D.J. McClements, H. Xiao, Is nano safe in foods? Establishing the factors impacting the gastrointestinal fate and toxicity of organic and inorganic food-grade nanoparticles, npj Science of Food 1(1) (2017) 6.
[19] T.B. Wagoner, E.A. Foegeding, Whey protein–pectin soluble complexes for beverage applications, Food Hydrocolloids 63 (2017) 130-138.
[20] A.B. Perumal, R.B. Nambiar, P.S. Sellamuthu, E.R. Sadiku, Application of Biosynthesized Nanoparticles in Food, Food Packaging and Dairy Industries, Biological Synthesis of Nanoparticles and Their Applications (2020) 145.
[21] M. Semenova, Protein–polysaccharide associative interactions in the design of tailor-made colloidal particles, Current opinion in colloid & interface science 28 (2017) 15-21.
[22] Q. Zhang, L. Li, Q. Lan, M. Li, D. Wu, H. Chen, Y. Liu, D. Lin, W. Qin, Z. Zhang, J. Liu, W. Yang, Protein glycosylation: a promising way to modify the functional properties and extend the application in food system, Critical Reviews in Food Science and Nutrition (2018) 1-28.
[23] D. Zhao, L. Li, T.T. Le, L.B. Larsen, D. Xu, W. Jiao, B. Sheng, B. Li, X. Zhang, Digestibility of glycated milk proteins and the peptidomics of their in vitro digests, Journal of the Science of Food and Agriculture 99(6) (2019) 3069-3077.
[24] A. Araiza-Calahorra, A. Sarkar, Designing biopolymer-coated Pickering emulsions to modulate in vitro gastric digestion: a static model study, Food & Function 10(9) (2019) 5498-5509.
[25] A. Sarkar, S. Zhang, B. Murray, J.A. Russell, S. Boxal, Modulating in vitro gastric digestion of emulsions using composite whey protein-cellulose nanocrystal interfaces, Colloids and Surfaces B: Biointerfaces 158 (2017) 137-146.
[26] M. Jiménez-Salcedo, M.T. Tena, Determination of cinnamaldehyde, carvacrol and thymol in feedstuff additives by pressurized liquid extraction followed by gas chromatography–mass spectrometry, Journal of Chromatography A 1487 (2017) 14-21.

[27] T. Niaz, S. Shabbir, T. Noor, A. Rahman, H. Bokhari, M. Imran, Potential of polymer stabilized nano-liposomes to enhance antimicrobial activity of nisin Z against foodborne pathogens, LWT 96 (2018) 98-110.
[28] G.H. Shin, J.T. Kim, Observation of chitosan coated lipid nanoparticles with different lipid compositions under simulated in vitro digestion system, Food Hydrocolloids 84 (2018) 146-153.
[29] D. Di Silvio, N. Rigby, B. Bajka, A. Mackie, F. Baldelli Bombelli, Effect of protein corona magnetite nanoparticles derived from bread in vitro digestion on Caco-2 cells morphology and uptake, The International Journal of Biochemistry & Cell Biology 75 (2016) 212-222.
[30] Y. Wei, S. Yang, L. Zhang, L. Dai, K. Tai, J. Liu, L. Mao, F. Yuan, Y. Gao, A. Mackie, Fabrication, characterization and in vitro digestion of food grade complex nanoparticles for co-delivery of resveratrol and coenzyme Q10, Food Hydrocolloids 105 (2020) 105791.
[31] M. Minekus, M. Alminger, P. Alvito, S. Ballance, T. Bohn, C. Bourlieu, F. Carriere, R. Boutrou, M. Corredig, D. Dupont, A standardised static in vitro digestion method suitable for food–an international consensus, Food & function 5(6) (2014) 1113-1124.
[32] L. Egger, O. Ménard, C. Delgado-Andrade, P. Alvito, R. Assunção, S. Balance, R. Barberá, A. Brodkorb, T. Cattenoz, A. Clemente, The harmonized INFOGEST in vitro digestion method: From knowledge to action, Food Research International 88 (2016) 217-225.
[33] S. Oh, M. Wilcox, J.P. Pearson, S. Borrós, Optimal design for studying mucoadhesive polymers interaction with gastric mucin using a quartz crystal microbalance with dissipation (QCM-D): Comparison of two different mucin origins, European Journal of Pharmaceutics and Biopharmaceutics 96 (2015) 477-483.
[34] S. Oh, S. Borrós, Mucoadhesion vs mucus permeability of thiolated chitosan polymers and their resulting nanoparticles using a quartz crystal microbalance with dissipation (QCM-D), Colloids and Surfaces B: Biointerfaces 147 (2016) 434-441.
[35] F. Xu, E. Liamas, M. Bryant, A.F. Adedeji, E. Andablo-Reyes, M. Castronovo, R. Ettelaie, T.V. Charpentier, A. Sarkar, A Self-Assembled Binary Protein Model Explains High-Performance Salivary Lubrication from Macro to Nanoscale, Advanced Materials Interfaces 7(1) (2020) 1901549.
[36] R.C.G. Corrêa, C.W.I. Haminiuk, L. Barros, M.I. Dias, R.C. Calhelha, C.G. Kato, V.G. Correa, R.M. Peralta, I.C.F.R. Ferreira, Stability and biological activity of Merlot (Vitis vinifera) grape pomace phytochemicals after simulated in vitro gastrointestinal digestion and colonic fermentation, Journal of Functional Foods 36 (2017) 410-417.

[37] A. Marchese, E. Coppo, A.P. Sobolev, D. Rossi, L. Mannina, M. Daglia, Influence of in vitro simulated gastroduodenal digestion on the antibacterial activity, metabolic profiling and polyphenols content of green tea (Camellia sinensis), Food Research International 63 (2014) 182-191.

[38] J. Yang, O.N. Ciftci, Development of free-flowing peppermint essential oil-loaded hollow solid lipid micro- and nanoparticles via atomization with carbon dioxide, Food Research International 87 (2016) 83-91.

[39] P. Shinde, H. Agraval, A.K. Srivastav, U.C. Yadav, U. Kumar, Physico-chemical characterization of carvacrol loaded zein nanoparticles for enhanced anticancer activity and investigation of molecular interactions between them by molecular docking, International Journal of Pharmaceutics 588 (2020) 119795.

[40] M.G. Ghahfarokhi, M. Barzegar, M. Sahari, M. Azizi, Enhancement of thermal stability and antioxidant activity of thyme essential oil by encapsulation in chitosan nanoparticles, J. Agric. Sci. Technol 18 (2016) 1781-1792.

[41] T. Niaz, S. Shabbir, T. Noor, R. Abbasi, Z.A. Raza, M. Imran, Polyelectrolyte multicomponent colloidosomes loaded with nisin Z for enhanced antimicrobial activity against foodborne resistant pathogens, Frontiers in microbiology 8 (2018) 2700.

[42] S.S. Rajan, A. PANDIAN, T. PALANIAPPAN, Curcumin loaded in bovine serum albumin–chitosan derived nanoparticles for targeted drug delivery, Bulletin of Materials Science 39(3) (2016) 811-817.

[43] I. Khan, A. Bahuguna, P. Kumar, V.K. Bajpai, S.C. Kang, In vitro and in vivo antitumor potential of carvacrol nanoemulsion against human lung adenocarcinoma A549 cells via mitochondrial mediated apoptosis, Scientific reports 8(1) (2018) 144.

[44] D. Sun, S. Kang, C. Liu, Q. Lu, L. Cui, B. Hu, Effect of zeta potential and particle size on the stability of SiO2 nanospheres as carrier for ultrasound imaging contrast agents, Int. J. Electrochem. Sci 11(10) (2016) 8520-8529.

[45] R.D. Koyani, M. Andrade, K. Quester, P. Gaytán, A. Huerta-Saquero, R. Vazquez-Duhalt, Surface modification of protein enhances encapsulation in chitosan nanoparticles, Applied Nanoscience 8(5) (2018) 1197-1203.

[46] A.O. Elzoghby, W.M. Samy, N.A. Elgindy, Albumin-based nanoparticles as potential controlled release drug delivery systems, Journal of Controlled Release 157(2) (2012) 168-182.

[47] S. Gaur, E.C. Lopez, A. Ojha, J.E. Andrade, Functionalization of Lipid-Based Nutrient Supplement with β-Cyclodextrin Inclusions of Oregano Essential Oil, Journal of Food Science 83(6) (2018) 1748-1756.

[48] S.F. Hosseini, M. Rezaei, M. Zandi, F. Farahmandghavi, Development of bioactive fish gelatin/chitosan nanoparticles composite films with antimicrobial properties, Food Chemistry 194 (2016) 1266-1274.
[49] J.J. Joseph, D. Sangeetha, T. Gomathi, Sunitinib loaded chitosan nanoparticles formulation and its evaluation, International Journal of Biological Macromolecules 82 (2016) 952-958.
[50] A. Esmaeili, A. Asgari, In vitro release and biological activities of Carum copticum essential oil (CEO) loaded chitosan nanoparticles, International Journal of Biological Macromolecules 81 (2015) 283-290.
[51] X. Zou, X. Zhao, L. Ye, Q. Wang, H. Li, Preparation and drug release behavior of pH-responsive bovine serum albumin-loaded chitosan microspheres, Journal of Industrial and Engineering Chemistry 21 (2015) 1389-1397.
[52] B.R. Shah, Y. Li, W. Jin, Y. An, L. He, Z. Li, W. Xu, B. Li, Preparation and optimization of Pickering emulsion stabilized by chitosan-tripolyphosphate nanoparticles for curcumin encapsulation, Food Hydrocolloids 52 (2016) 369-377.
[53] L.B. Rodriguez, A. Avalos, N. Chiaia, A. Nadarajah, Effect of formulation and process parameters on chitosan microparticles prepared by an emulsion crosslinking technique, AAPS PharmSciTech 18(4) (2017) 1084-1094.
[54] J.K. de Oliveira, D.F. Ronik, J. Ascari, R.M. Mainardes, N.M. Khalil, Nanoencapsulation of Apocynin in Bovine Serum Albumin Nanoparticles: Physicochemical Characterization, Nanoscience & Nanotechnology-Asia 8(1) (2018) 90-99.
[55] M. Ghorbani, H. Hamishehkar, M. Tabibiazar, BSA/Chitosan Polyelectrolyte Complex: A Platform for Enhancing the Loading and Cancer Cell-Uptake of Resveratrol, Macromolecular Research (2018) 1-6.
[56] G.G.G. Trindade, G. Thrivikraman, P.P. Menezes, C.M. França, B.S. Lima, Y.M.B.G. Carvalho, E.P.B.S.S. Souza, M.C. Duarte, S. Shanmugam, L.J. Quintans-Júnior, D.P. Bezerra, L.E. Bertassoni, A.A.S. Araújo, Carvacrol/β-cyclodextrin inclusion complex inhibits cell proliferation and migration of prostate cancer cells, Food and Chemical Toxicology 125 (2019) 198-209.
[57] L. Keawchaoon, R. Yoksan, Preparation, characterization and in vitro release study of carvacrol-loaded chitosan nanoparticles, Colloids and Surfaces B: Biointerfaces 84(1) (2011) 163-171.
[58] K.I. Matshetshe, S. Parani, S.M. Manki, O.S. Oluwafemi, Preparation, characterization and in vitro release study of β-cyclodextrin/chitosan nanoparticles loaded Cinnamomum

731 zeylanicum essential oil, International Journal of Biological Macromolecules 118 (2018) 676-
732 682.
733 [59] R. Li, Z. Wu, Y. Wangb, L. Ding, Y. Wang, Role of pH-induced structural change in
734 protein aggregation in foam fractionation of bovine serum albumin, Biotechnology Reports 9
735 (2016) 46-52.
736 [60] T. Niaz, A. Ihsan, R. Abbasi, S. Shabbir, T. Noor, M. Imran, Chitosan-albumin based core
737 shell-corona nano-antimicrobials to eradicate resistant gastric pathogen, International Journal
738 of Biological Macromolecules (2019).
739 [61] L.R. Barbosa, M.G. Ortore, F. Spinozzi, P. Mariani, S. Bernstorff, R. Itri, The importance
740 of protein-protein interactions on the pH-induced conformational changes of bovine serum
741 albumin: a small-angle X-ray scattering study, Biophysical journal 98(1) (2010) 147-157.
742 [62] W. Liu, Y. Kong, P. Tu, J. Lu, C. Liu, W. Liu, J. Han, J. Liu, Physical–chemical stability
743 and in vitro digestibility of hybrid nanoparticles based on the layer-by-layer assembly of
744 lactoferrin and BSA on liposomes, Food & Function 8(4) (2017) 1688-1697.
745 [63] Z.-W. Jing, Y.-Y. Jia, N. Wan, M. Luo, M.-L. Huan, T.-B. Kang, S.-Y. Zhou, B.-L. Zhang,
746 Design and evaluation of novel pH-sensitive ureido-conjugated chitosan/TPP nanoparticles
747 targeted to Helicobacter pylori, Biomaterials 84 (2016) 276-285.
748 [64] A. Moeini, A. Cimmino, G. Dal Poggetto, M. Di Biase, A. Evidente, M. Masi, P.
749 Lavermicocca, F. Valerio, A. Leone, G. Santagata, M. Malinconico, Effect of pH and TPP
750 concentration on chemico-physical properties, release kinetics and antifungal activity of
751 Chitosan-TPP-Ungeremine microbeads, Carbohydrate Polymers 195 (2018) 631-641.
752 [65] L. Dai, R. Li, Y. Wei, C. Sun, L. Mao, Y. Gao, Fabrication of zein and rhamnolipid
753 complex nanoparticles to enhance the stability and in vitro release of curcumin, Food
754 Hydrocolloids 77 (2018) 617-628.
755 [66] T. M Ways, W. Lau, V. Khutoryanskiy, Chitosan and its derivatives for application in
756 mucoadhesive drug delivery systems, Polymers 10(3) (2018) 267.
757 [67] A.C. Vieira, L.L. Chaves, S. Pinheiro, S. Pinto, M. Pinheiro, S.C. Lima, D. Ferreira, B.
758 Sarmento, S. Reis, Mucoadhesive chitosan-coated solid lipid nanoparticles for better
759 management of tuberculosis, International Journal of Pharmaceutics 536(1) (2018) 478-485.
760 [68] Z.-P. Zhao, Z. Wang, S.-C. Wang, Formation, charged characteristic and BSA adsorption
761 behavior of carboxymethyl chitosan/PES composite MF membrane, Journal of Membrane
762 Science 217(1-2) (2003) 151-158.
763 [69] M. Lopes, N. Shrestha, A. Correia, M.-A. Shahbazi, B. Sarmento, J. Hirvonen, F. Veiga,
764 R. Seiça, A. Ribeiro, H.A. Santos, Dual chitosan/albumin-coated alginate/dextran sulfate

765 nanoparticles for enhanced oral delivery of insulin, Journal of Controlled Release 232 (2016)
766 29-41.
767 [70] D. Pauluk, A.K. Padilha, N.M. Khalil, R.M. Mainardes, Chitosan-coated zein
768 nanoparticles for oral delivery of resveratrol: Formation, characterization, stability,
769 mucoadhesive properties and antioxidant activity, Food Hydrocolloids 94 (2019) 411-417.
770 [71] M. Arif, Q.-J. Dong, M.A. Raja, S. Zeenat, Z. Chi, C.-G. Liu, Development of novel pH-
771 sensitive thiolated chitosan/PMLA nanoparticles for amoxicillin delivery to treat Helicobacter
772 pylori, Materials Science and Engineering: C 83 (2018) 17-24.
773 [72] A.F. Esfanjani, E. Assadpour, S.M. Jafari, Improving the bioavailability of phenolic
774 compounds by loading them within lipid-based nanocarriers, Trends in Food Science &
775 Technology 76 (2018) 56-66.
776 [73] S.M.T. Gharibzahedi, S. Mohammadnabi, Characterizing the novel surfactant-stabilized
777 nanoemulsions of stinging nettle essential oil: Thermal behaviour, storage stability,
778 antimicrobial activity and bioaccessibility, Journal of Molecular Liquids 224 (2016) 1332-
779 1340.
780 [74] A. Sarkar, A. Ye, H. Singh, On the role of bile salts in the digestion of emulsified lipids,
781 Food Hydrocolloids 60 (2016) 77-84.
782 [75] S. Nowotarska, K. Nowotarski, I. Grant, C. Elliott, M. Friedman, C. Situ, Mechanisms of
783 antimicrobial action of cinnamon and oregano oils, cinnamaldehyde, carvacrol, 2, 5-
784 dihydroxybenzaldehyde, and 2-hydroxy-5-methoxybenzaldehyde against Mycobacterium
785 avium subsp. paratuberculosis (Map), Foods 6(9) (2017) 72.
786 [76] W. Lim, J. Ham, F.W. Bazer, G. Song, Carvacrol induces mitochondria-mediated
787 apoptosis via disruption of calcium homeostasis in human choriocarcinoma cells, Journal of
788 Cellular Physiology 234(2) (2019) 1803-1815.

789

Figure captions:

Figure 1: Mean particle size determined by dynamic light scattering (A), zeta-potential (B) of core and corona modified CS-NDS with or without carvacrol and (C) encapsulation efficiency (%EE) as a function of physiologically-relevant pH values.

Figure 2: Morphological evaluation of fabricated nano delivery systems including void chitosan NDS (I), carvacrol-loaded chitosan NDS (II and III), void BSA-CS-NDS (IV) and carvacrol-loaded BSA-CS-NDS (V and VI) performed by scanning electron microscopy (SEM).

Figure 3: Fourier transform infrared spectra of BSA, CS and void BSA-CS NDS (I), void CS-NDS and carvacrol loaded CS-NDS (II), carvacrol and carvacrol-loaded BSA-CS-NDS (III).

Figure 4: Particle size of chitosan-based nano-formulation (A) and BSA-coated chitosan-based nano-formulation (B). Here (I, II) represent void nano delivery systems, whereas (III, IV) represent carvacrol-loaded nano delivery systems during gastric and intestinal digestion, respectively.

Figure 5: Zeta-potential of chitosan based nano-formulation and BSA-coated chitosan based nano-formulation. Here (I, II) represent void and loaded CS-NDS, whereas (III, IV) represent void and loaded BSA-CS core-corona NDS during gastric and intestinal digestion.

Figure 6: Release profile of carvacrol (CAR) in simulated gastrointestinal fluid from chitosan nano delivery systems (CS-NDS) (I) and BSA corona modified chitosan nano delivery systems (BSA-CS-NDS) (II).

Figure 7: Mucoadhesive studies of corona modified nano-systems were performed by quartz crystal microbalance with dissipation (QCM-D). Changes in frequency (Δf) and dissipation (ΔD) with time, represented by blue line and red line respectively, were recorded for chitosan nano delivery systems (A-I) and BSA-CS core-corona NDS (A-II) on mucin-coated crystals. The 5^{th} overtone is shown. Change in mass due to adsorption of unmodified CS-NDS and corona modified BSA-CS-NDS on mucin-coated surface (B) was measured at gastric pH i.e. pH 3.0. Statistical significance of the data was measured by one-way ANOVA test.

Figure 8: Antimicrobial potential of digested samples (at different time intervals) of carvacrol loaded corona modified BSA-CS-NDS and unmodified core CS-NDS in intestinal phase against *Salmonella enterica*. Average of the data (n=3) was plotted. Error bars represent (+/-) standard deviation. Statistical significance of the data was measured by T test (**$p < 0.01$, ***$p < 0.001$, **** $p < 0.0001$).

Figure 1

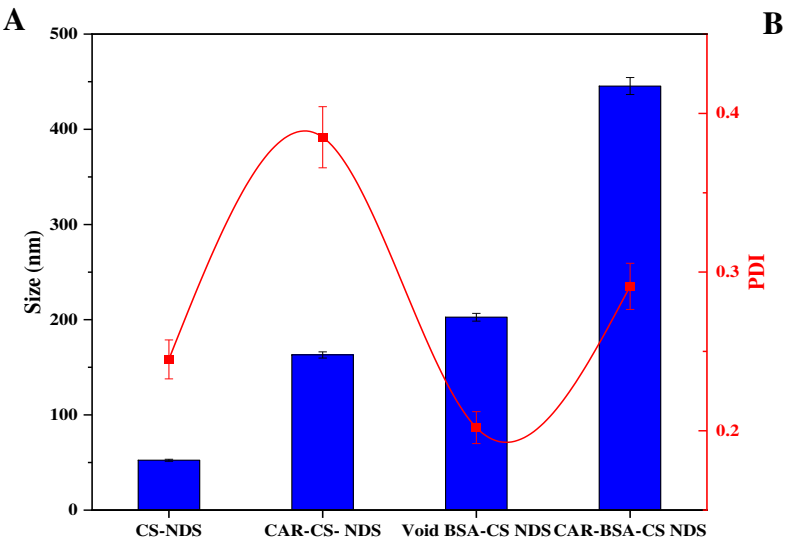
A
Size (nm)
PDI
CS-NDS
CAR-CS- NDS
Void BSA-CS NDS
CAR-BSA-CS NDS

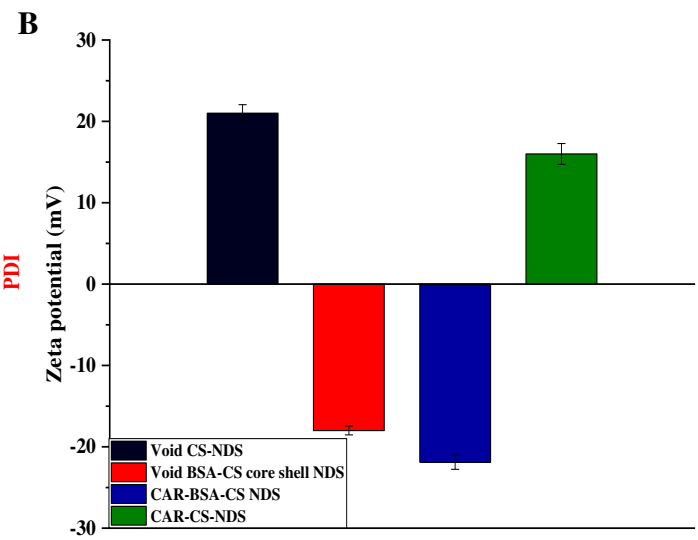
B
Zeta potential (mV)
Void CS-NDS
Void BSA-CS core shell NDS
CAR-BSA-CS NDS
CAR-CS-NDS

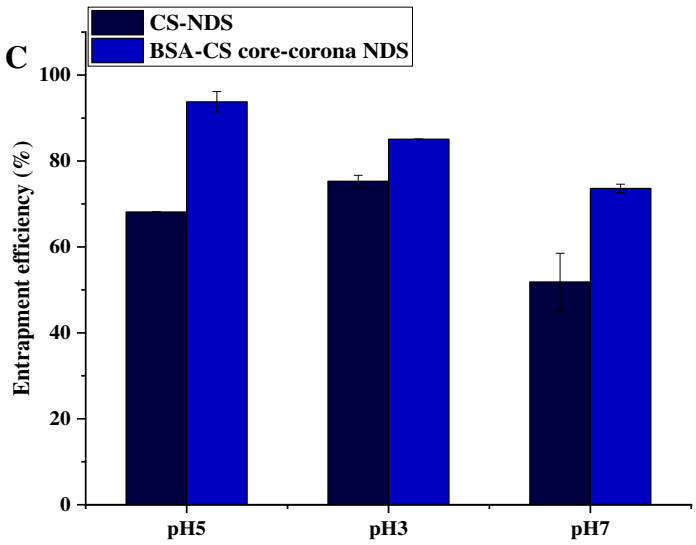
C
CS-NDS
BSA-CS core-corona NDS
Entrapment efficiency (%)
pH5
pH3
pH7

Figure 2

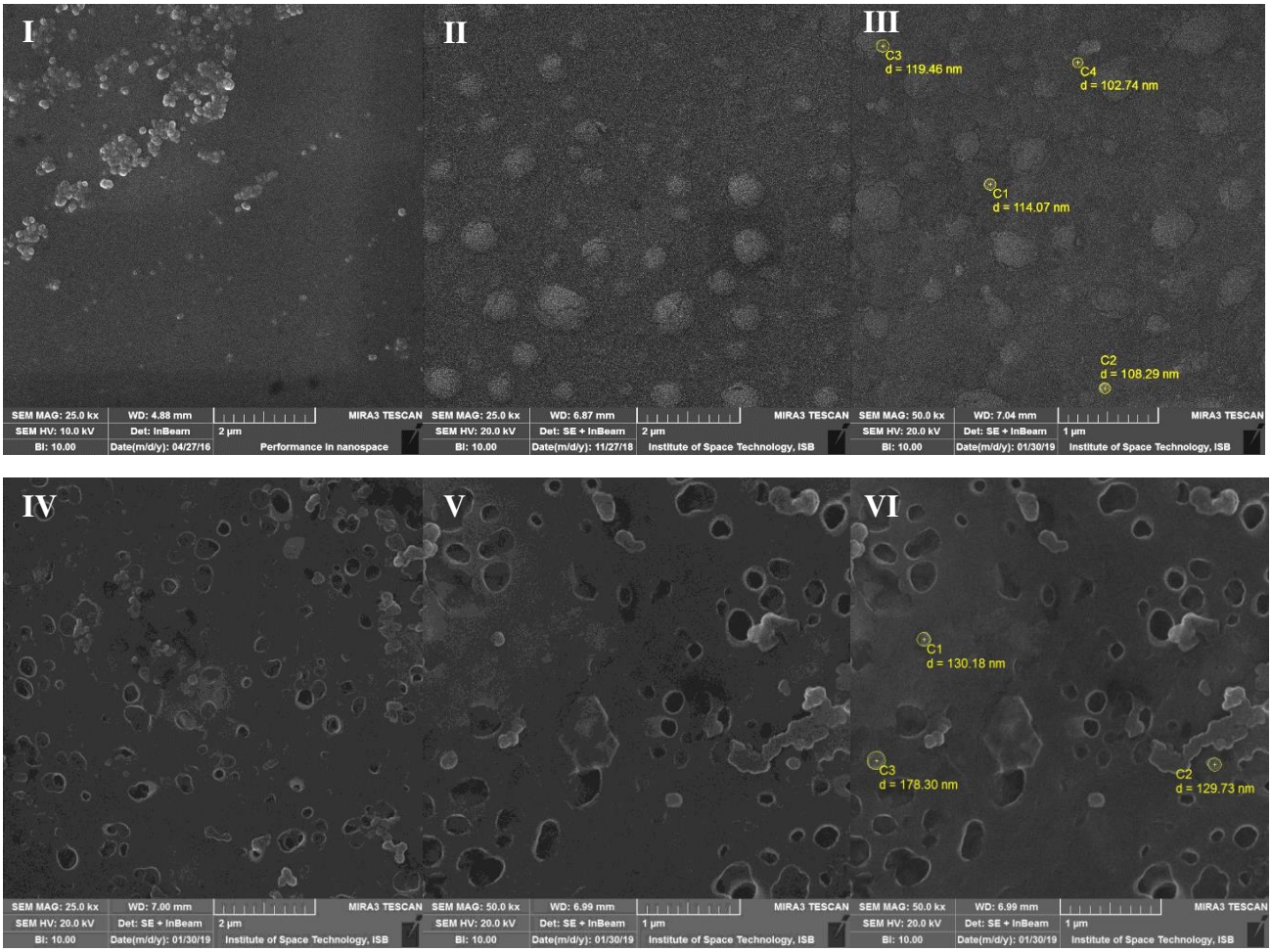
I
II
III
C3
d = 119.46 nm
C4
d = 102.74 nm
C1
d = 114.07 nm
C2
d = 108.29 nm
SEM MAG: 25.0 kx
WD: 4.88 mm
MIRA3 TESCAN
SEM HV: 10.0 kV
Det: InBeam
2 µm
BI: 10.00
Date(m/d/y): 04/27/16
Performance in nanospace
SEM MAG: 25.0 kx
WD: 6.87 mm
MIRA3 TESCAN
SEM HV: 20.0 kV
Det: SE + InBeam
2 µm
BI: 10.00
Date(m/d/y): 11/27/18
Institute of Space Technology, ISB
SEM MAG: 50.0 kx
WD: 7.04 mm
MIRA3 TESCAN
SEM HV: 20.0 kV
Det: SE + InBeam
1 µm
BI: 10.00
Date(m/d/y): 01/30/19
Institute of Space Technology, ISB
IV
V
VI
C1
d = 130.18 nm
C3
d = 178.30 nm
C2
d = 129.73 nm
SEM MAG: 25.0 kx
WD: 7.00 mm
MIRA3 TESCAN
SEM HV: 20.0 kV
Det: SE + InBeam
2 µm
BI: 10.00
Date(m/d/y): 01/30/19
Institute of Space Technology, ISB
SEM MAG: 50.0 kx
WD: 6.99 mm
MIRA3 TESCAN
SEM HV: 20.0 kV
Det: SE + InBeam
1 µm
BI: 10.00
Date(m/d/y): 01/30/19
Institute of Space Technology, ISB
SEM MAG: 50.0 kx
WD: 6.99 mm
MIRA3 TESCAN
SEM HV: 20.0 kV
Det: SE + InBeam
1 µm
BI: 10.00
Date(m/d/y): 01/30/19
Institute of Space Technology, ISB

Figure 3

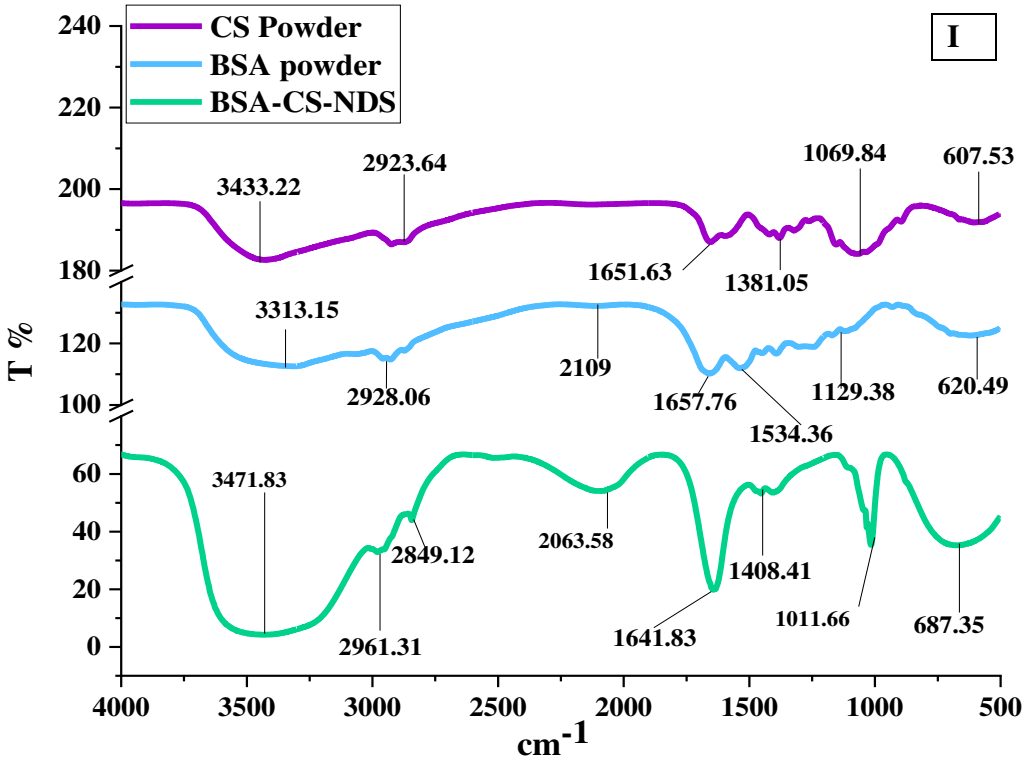
CS Powder
BSA powder
BSA-CS-NDS
I
T %
cm-1
3433.22
2923.64
1651.63
1381.05
1069.84
607.53
3313.15
2928.06
2109
1657.76
1534.36
1129.38
620.49
3471.83
2961.31
2849.12
2063.58
1641.83
1408.41
1011.66
687.35

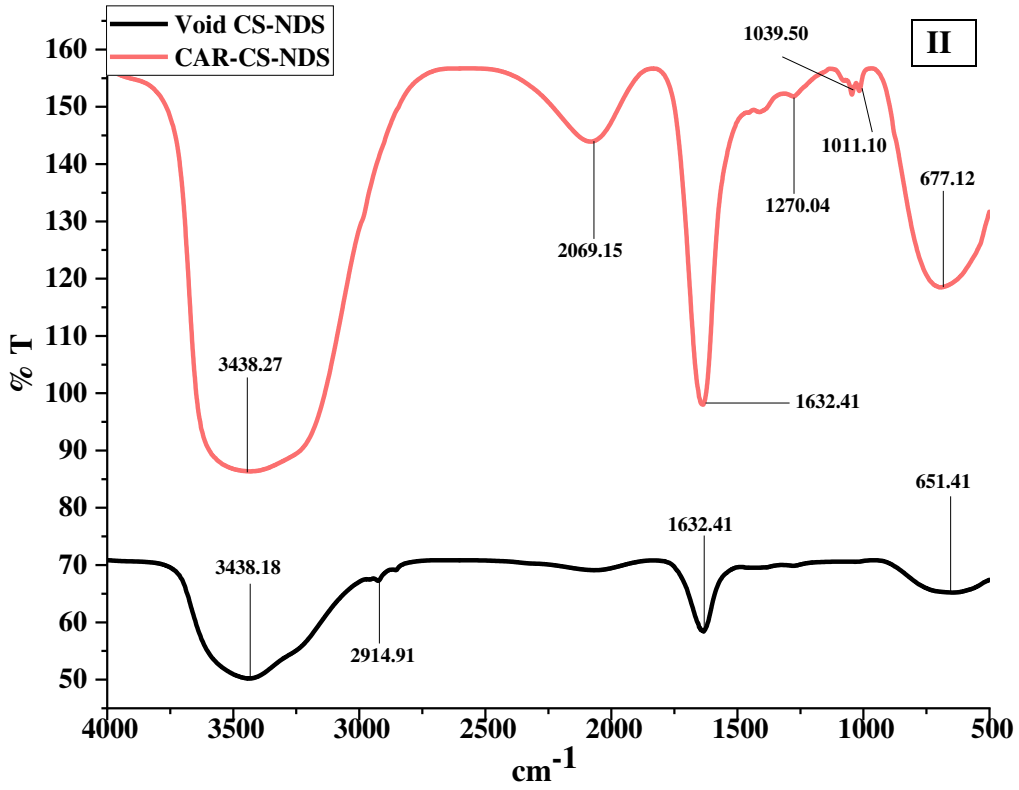
Void CS-NDS
CAR-CS-NDS
II
1039.50
1011.10
677.12
1270.04
2069.15
3438.27
1632.41
651.41
1632.41
3438.18
2914.91
% T
cm-1

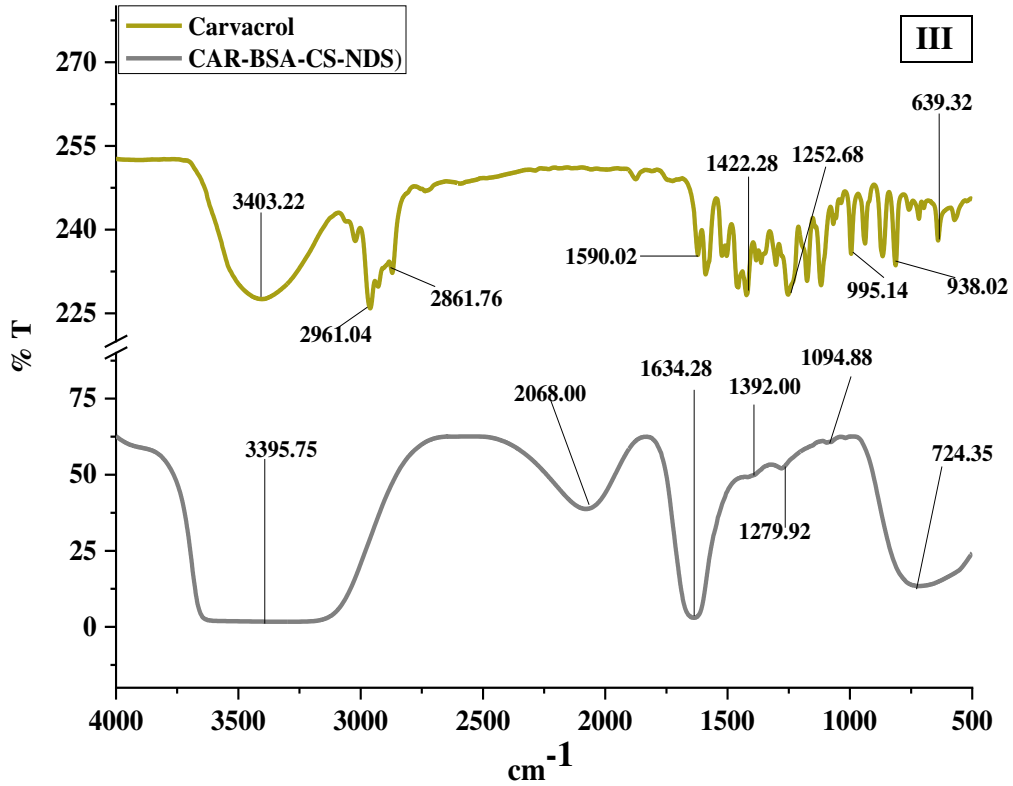
Carvacrol
CAR-BSA-CS-NDS)
III
639.32
1422.28
1252.68
3403.22
1590.02
2861.76
995.14
938.02
2961.04
1094.88
1634.28
1392.00
2068.00
3395.75
724.35
1279.92
% T
cm-1

Figure 4

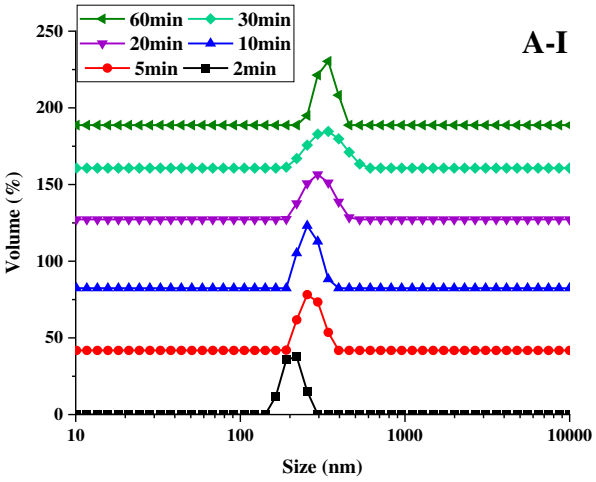
A-I
60min
30min
20min
10min
5min
2min
Volume (%)
Size (nm)
0
50
100
150
200
250
10
100
1000
10000

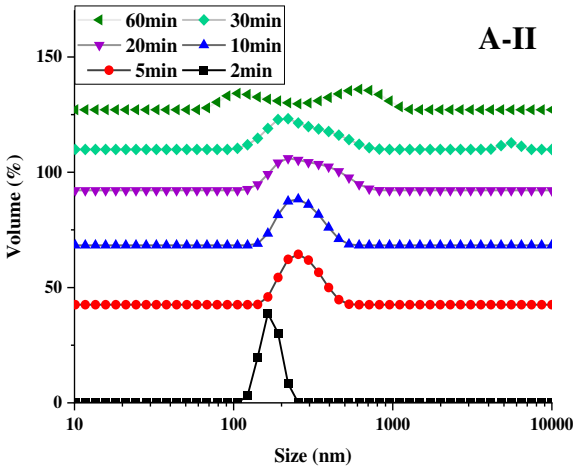
A-II
60min
30min
20min
10min
5min
2min
Volume (%)
Size (nm)
0
50
100
150
10
100
1000
10000

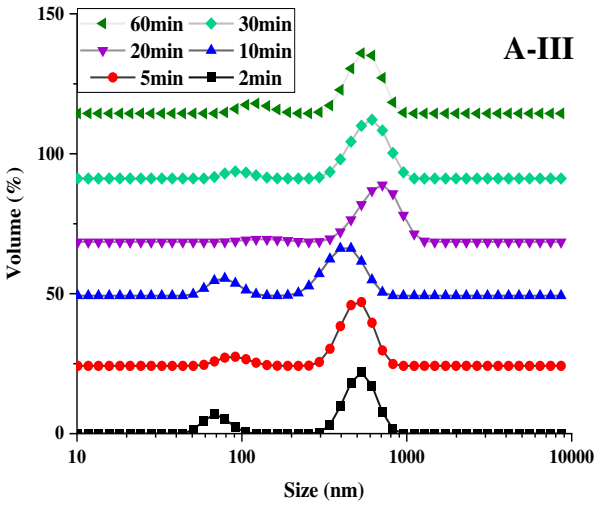
A-III
60min
30min
20min
10min
5min
2min
Volume (%)
Size (nm)
0
50
100
150
10
100
1000
10000

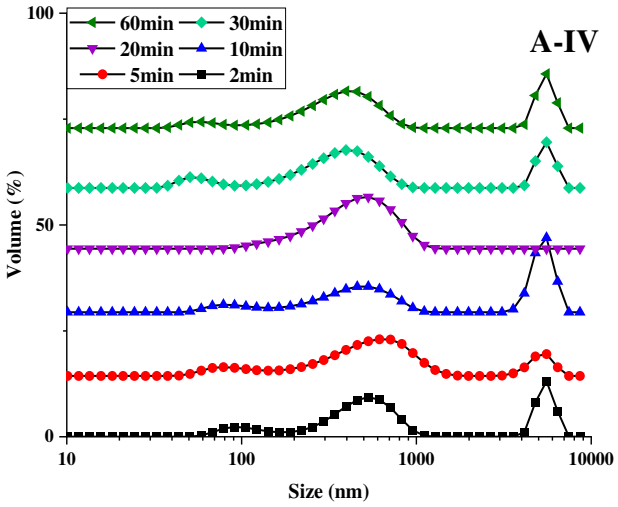
A-IV
60min
30min
20min
10min
5min
2min
Volume (%)
Size (nm)
0
50
100
10
100
1000
10000

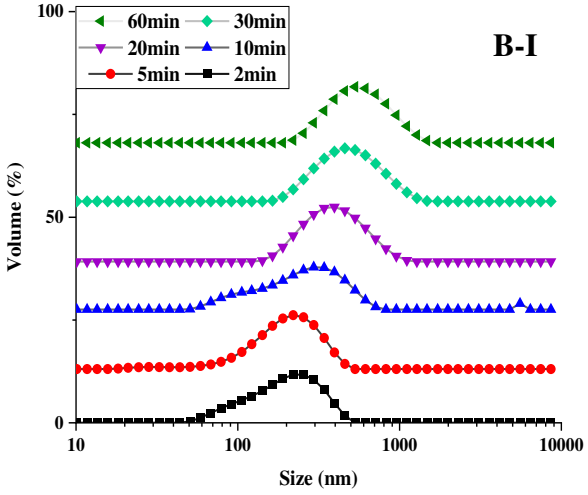
B-I
60min
30min
20min
10min
5min
2min
Volume (%)
Size (nm)
0
50
100
10
100
1000
10000

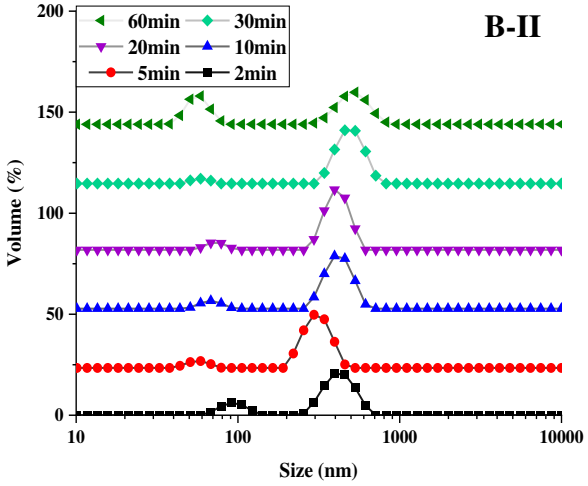
B-II
60min
30min
20min
10min
5min
2min
Volume (%)
Size (nm)
0
50
100
150
200
10
100
1000
10000

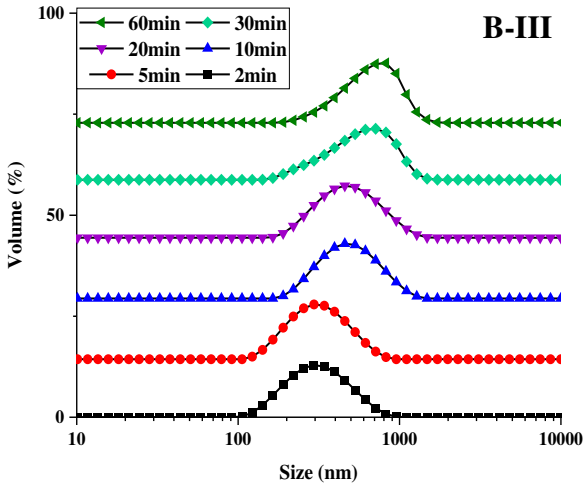
B-III
60min
30min
20min
10min
5min
2min
Volume (%)
Size (nm)
0
50
100
10
100
1000
10000

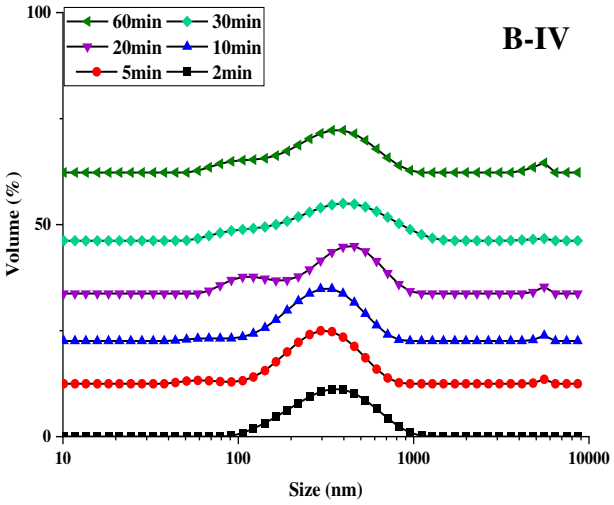
B-IV
60min
30min
20min
10min
5min
2min
Volume (%)
Size (nm)
0
50
100
10
100
1000
10000

Figure 5

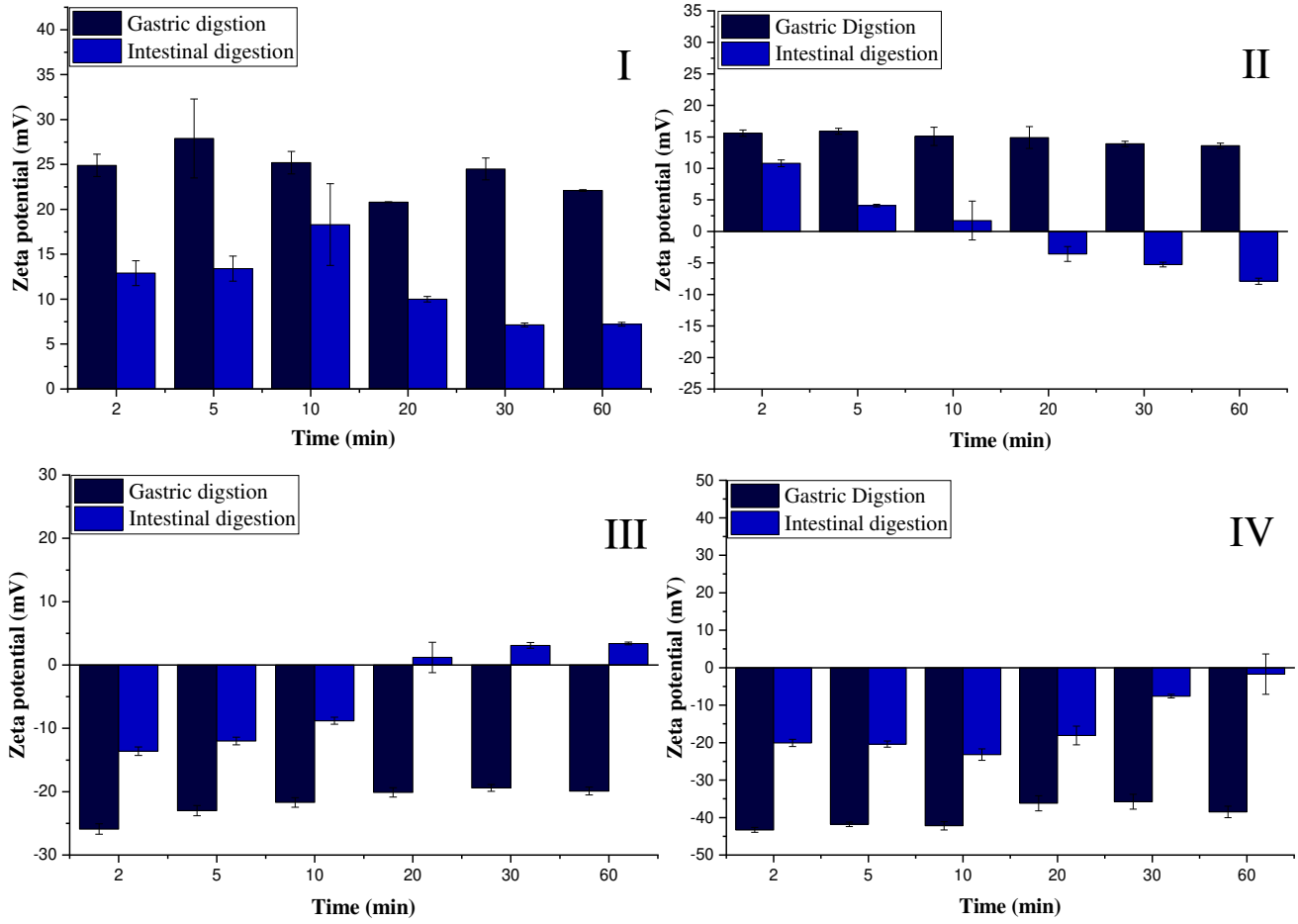
I
Gastric digstion
Intestinal digestion
Zeta potential (mV)
Time (min)
II
Gastric Digstion
Intestinal digestion
Zeta potential (mV)
Time (min)
III
Gastric digstion
Intestinal digestion
Zeta potential (mV)
Time (min)
IV
Gastric Digstion
Intestinal digestion
Zeta potential (mV)
Time (min)

Figure 6

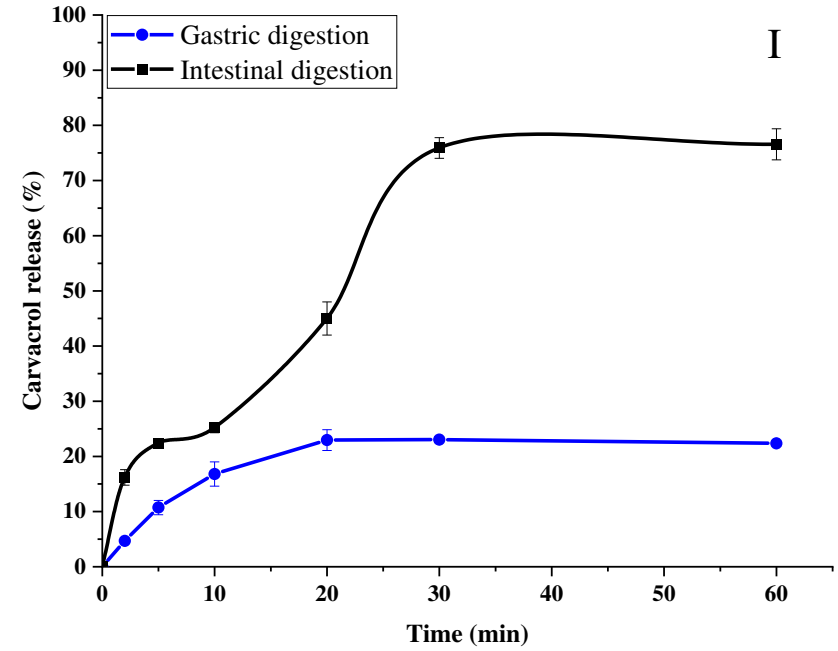
I
Gastric digestion
Intestinal digestion
Carvacrol release (%)
Time (min)
0
10
20
30
40
50
60
70
80
90
100

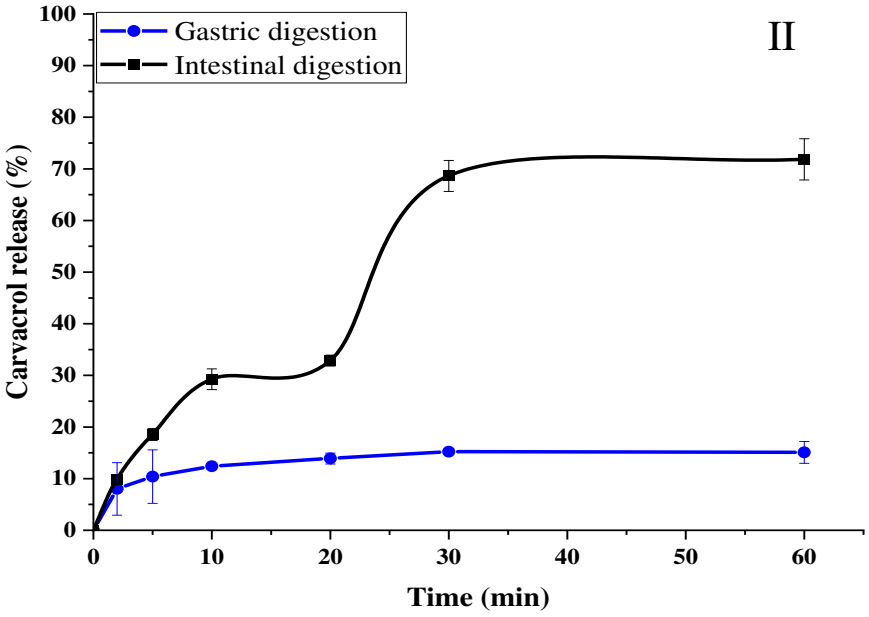
II
Gastric digestion
Intestinal digestion
Carvacrol release (%)
Time (min)
0
10
20
30
40
50
60
70
80
90
100

Figure 7

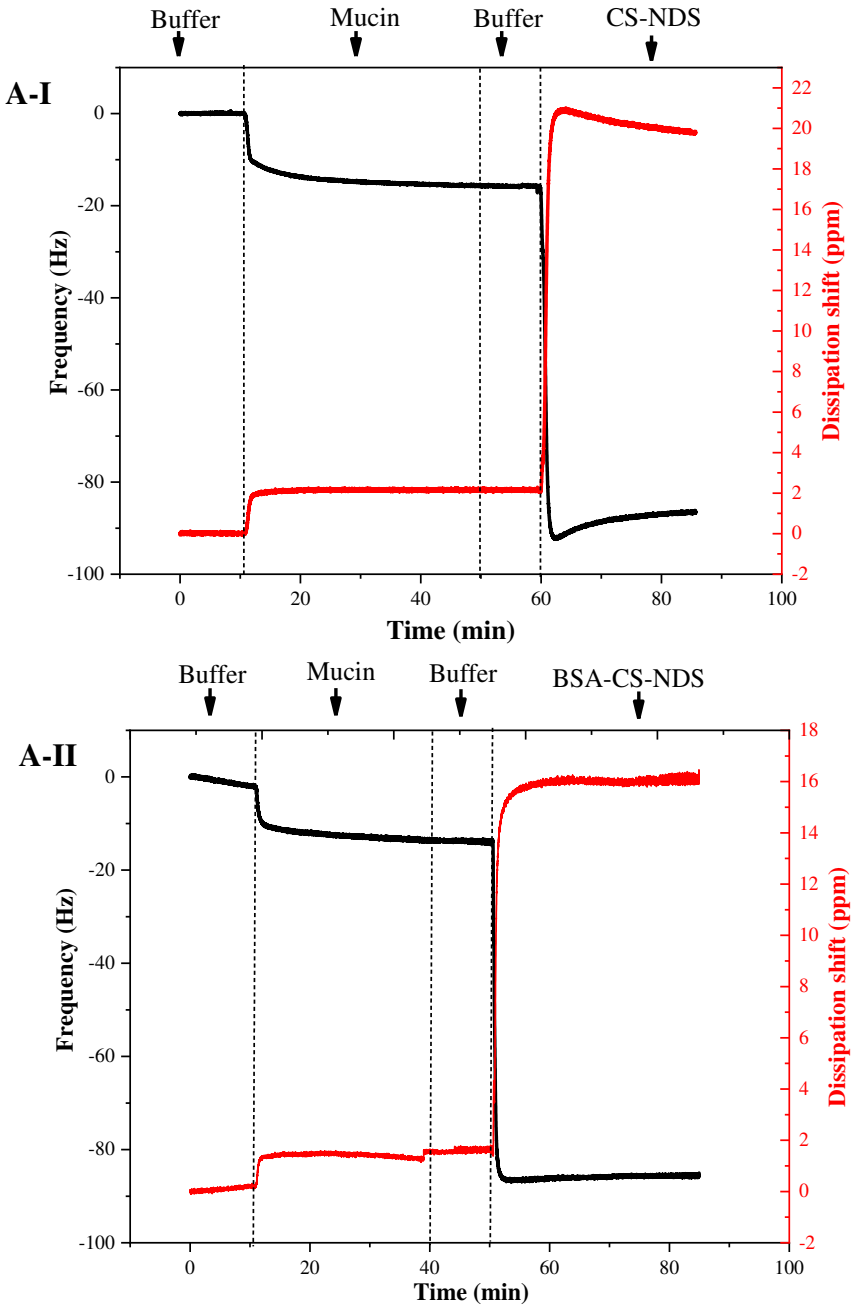
A-I
Buffer
Mucin
Buffer
CS-NDS
Frequency (Hz)
Dissipation shift (ppm)
Time (min)
A-II
Buffer
Mucin
Buffer
BSA-CS-NDS
Frequency (Hz)
Dissipation shift (ppm)
Time (min)

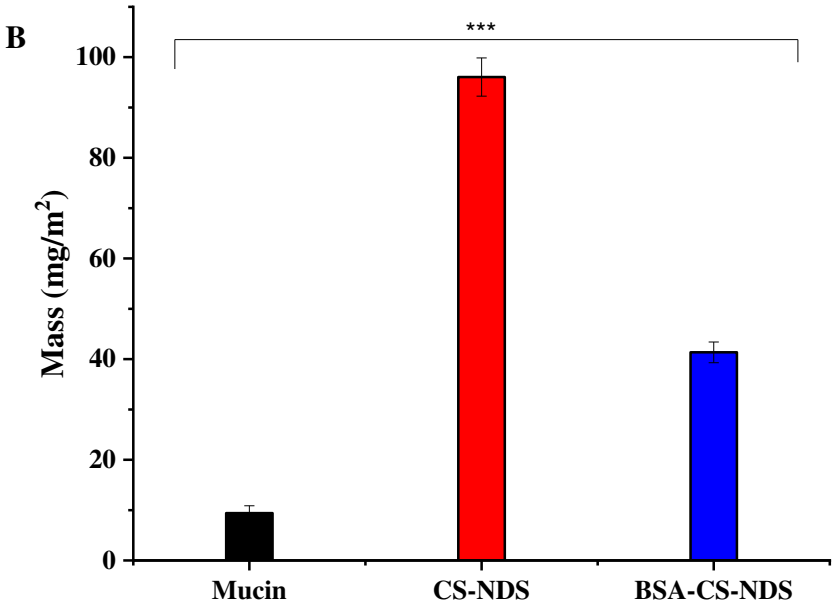
B
***
100
80
60
40
20
0
Mass (mg/m2)
Mucin
CS-NDS
BSA-CS-NDS

Figure 8

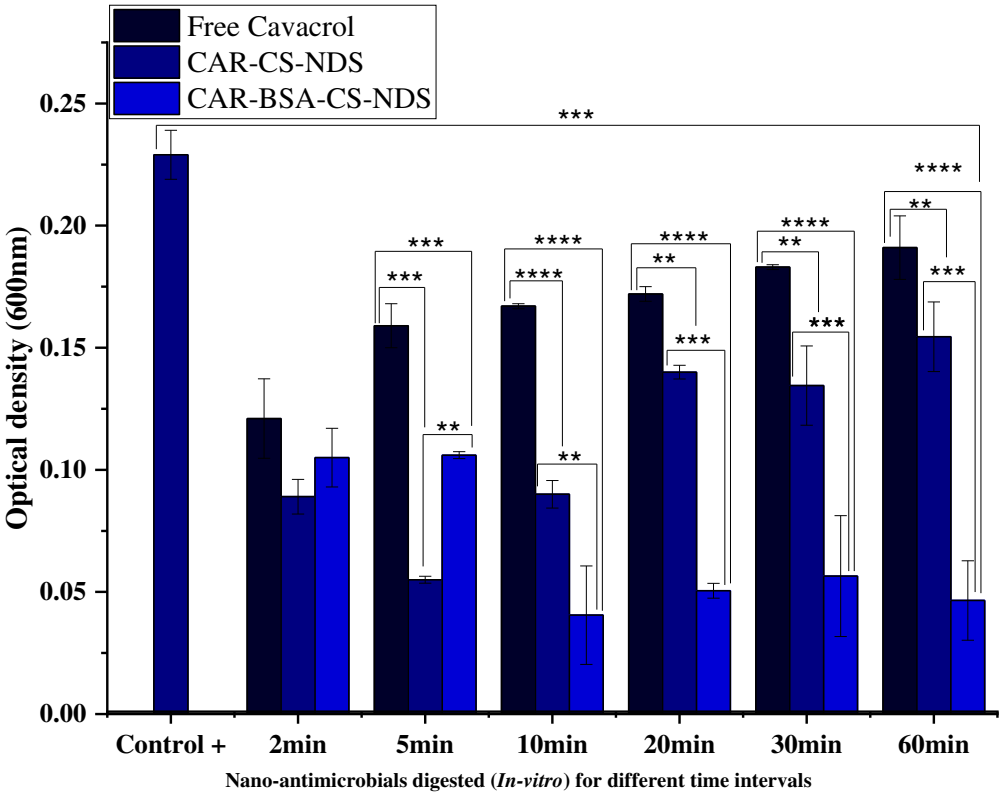
Free Cavacrol
CAR-CS-NDS
CAR-BSA-CS-NDS
Optical density (600nm)
0.00
0.05
0.10
0.15
0.20
0.25
Control +
2min
5min
10min
20min
30min
60min
Nano-antimicrobials digested (*In-vitro*) for different time intervals

Supplementary data

Figure S1: In vitro cell viability of free carvacrol, carvacrol loaded core-CS-NDS as well as corona modified NDS in HepG2 cells after 24 h of treatment. Control cells were left untreated. The cell growth data shows mean ± SD (n = 3); signifying **p < 0.01, ***p < 0.0001.

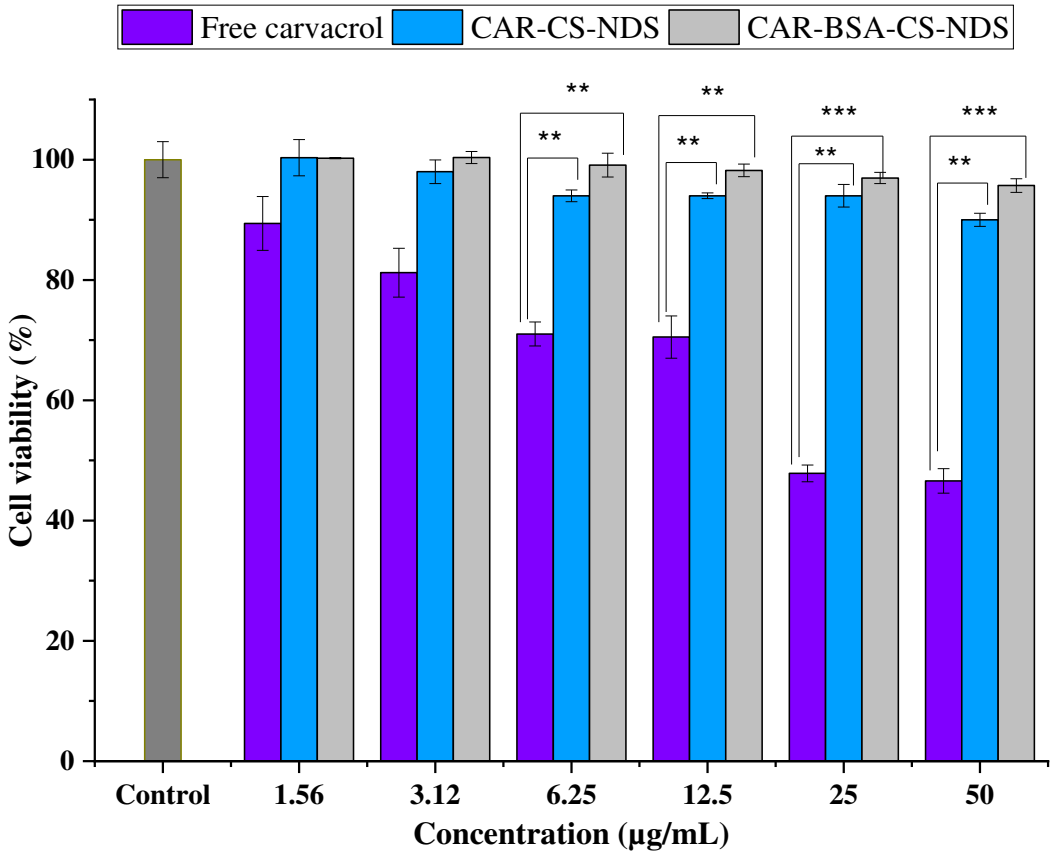

Graphical Abstract:

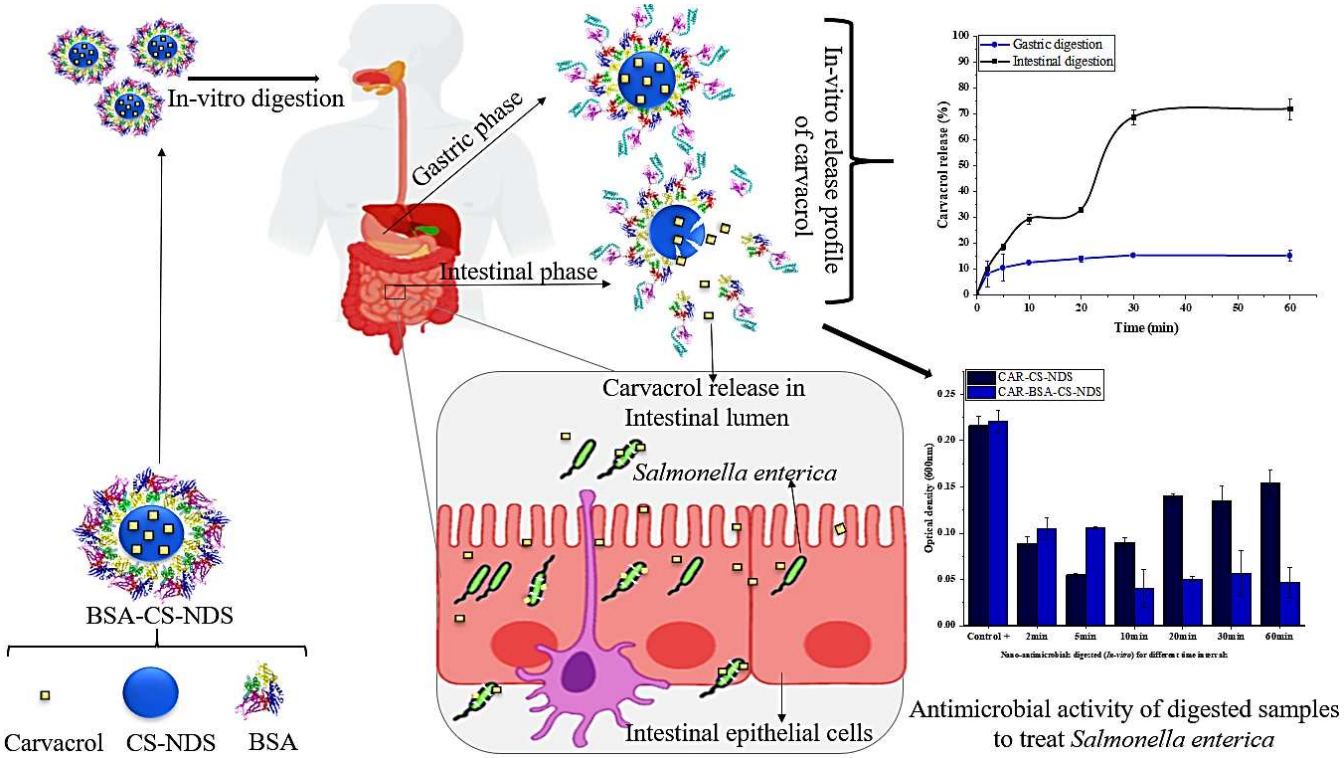

Highlights

- Corona modified NDS were developed for the sustained delivery of carvacrol in the intestine
- NDS of chitosan core having BSA corona were developed by ionic gelation and ultrasonication
- Corona modified nano-delivery systems increased the particle stability during *in vitro* digestion
- BSA-CS-NDS enabled a higher release of carvacrol in the intestinal phase
- Core-corona nano-antimicrobials successfully inhibited enteric pathogen i.e. *Salmonella enterica*